THE ASTROPHYSICAL JOURNAL, 443:586–605, 1995 April 20

THE ABSORPTION SPECTRUM OF NUCLEAR GAS IN Q0059−2735

E. JOSEPH WAMPLER,[1] NIKOLAI N. CHUGAI,[1,2] AND PATRICK PETITJEAN[1,3]
Received 1994 May 2; accepted 1994 October 25

ABSTRACT

Spectra of the broad absorption line (BAL) quasar Q0059−2735 taken with spectral resolutions of 10 and 20 km s^{-1} show that the absorption lines can be understood as a BAL flow together with low-ionization condensations. The condensations produce narrow ($b \lesssim 20$ km s^{-1}), saturated lines that fail to occult completely the central continuum sources or the low-ionization emission-line sources. Many of the narrow absorption lines (NAL) originate from metastable levels that lie several electron volts above the ground term. The level populations imply excitation temperatures of $\sim 10^4$ K. These levels may be populated either by collisional or radiative processes. Models show that the NAL gas lies a few parsecs from the central source.

The BAL absorption is much deeper than the NAL absorption. The high-ionization BAL flow must occult most of the quasar nucleus, but the shapes of the low-ionization BAL absorption troughs show that while the low-ionization BAL gas occults the nuclear continuum sources it fails to occult the low-ionization broad emission line region. Compared to the NAL clouds, the BAL clouds have a higher excitation temperature, ranging up to 6×10^4 K.

All these observed facts can be explained by a model in which low-ionization gas condensations lying above an accretion disk are being ablated by the intense radiation field of the quasar nucleus. The low-ionization condensations and the BAL flow occult different parts of the background emission regions. The origin of the low-ionization clouds is uncertain: they could be ablating stellar atmospheres, as suggested by Baldwin et al. (1993), or stand-off shocks around obstacles in a hot, supersonic flow of low-density gas from the central QSO nucleus (Perry & Dyson 1985), or they could be dense gas clouds, ejected by a supernova explosion (Artymowicz, Lin, & Wampler 1993) or, possibly, by instabilities in the accretion disk.

Subject headings: quasars: absorption lines — quasars: individual (Q0059−2735)

1. INTRODUCTION

Q0059−2735 is a member of the comparatively rare class of broad absorption line (BAL) quasars with strong BAL absorption from low-ionization lines such as Si II, Mg II, and Al II. It was identified and first studied by Hazard et al. (1987), who found that, in addition to the low-ionization BAL flow, the spectrum of Q0059−2735 contained many narrow absorption lines (NAL) from iron-peak elements. Present in the narrow-line spectrum are many absorption transitions from metastable levels that lie several electron volts above the ground term. These show that the narrow-line spectrum is closely associated with the quasar nucleus, and they make Q0059−2735 unique among known BAL quasars. No other BAL quasar has yet been found with strong, narrow, low-ionization lines associated with the quasar. Later, Voit, Weymann, & Korista (1993) modeled the Q0059−2735 BAL region. Both Hazard et al. (1987) and Voit et al. (1993) used low to moderate resolution spectra for their studies.

Using spectra taken with a spectral resolution that ranges from 10 to 20 km s^{-1}, we give a detailed analysis of the absorption spectrum of Q0059−2735. We find that all the observed absorption features, the narrow lines together with the BAL flow, result from quite simple cloud structures. It is remarkable that over 1000 narrow lines in the spectrum of Q0059−2735 can be modeled by assuming only four discrete cloud velocities with individual b-values of ~ 20 km s^{-1}. The BAL flow requires an additional nine cloud velocities with individual b-values that range from ~ 80 up to 400 km s^{-1}.

2. OBSERVATIONS

The spectra described here were obtained using ESO's two cross-dispersed echelle spectrographs: CASPEC on the 3.6 m telescope, and EMMI on the New Technology Telescope (NTT). An observing log is given in Table 1. The two spectrographs have complementary advantages. CASPEC has good response in the UV and blue-green wavelength region; EMMI has higher spectral resolution than CASPEC, but in its high-resolution mode it is only efficient at wavelengths longer than ~ 5000 Å. The CCD used with CASPEC had large pixels that undersampled the image plane; therefore, the maximum resolution achievable with CASPEC was about $R = \lambda/\Delta\lambda = 15{,}000$. About 2000 Å could be covered with one setting of the cross-disperser. EMMI can resolve $R = \lambda/\Delta\lambda = 30{,}000$ and can cover the wavelength interval from 6000 Å to 1 μm in one setting.

In the initial steps of the reduction procedure we first removed the low-frequency background, the night-sky lines, and the cosmic-ray events from the echelle image frames. The extraction procedure we used relies on the fact that neither the wavelength nor the intensity calibration nor the relative location of the echelle orders depends on the software offset of the extraction slit in the image plane. The ESO reduction package permits the operator to select a software extraction slit that is shorter than 1 pixel. We used an extraction slit height of $\frac{1}{3}$ pixel, and the extraction offsets were stepped in $\frac{1}{4}$ pixel steps from 10 pixels below the order centers to 10 pixels above the centers. Each extracted slice was then wavelength and intensity

[1] European Southern Observatory, Karl-Schwarzschild-Strasse 2, D-85748 Garching bei München, Germany.
[2] Postal address: Institute of Astronomy of the Russian Academy of Sciences, Pyatnitskaya 49, Moscow 109017, Russia.
[3] Postal address: Institut d'Astrophysique de Paris, 98b Boulevard Arago, 75014 Paris, France.

TABLE 1

OBSERVING LOG

Date (UT)	Instrument	Exposure (s)	λ_{ctr} (Å)
1990 Aug 22.....	CASPEC	7200	4300
1990 Aug 23.....	CASPEC	7200	4300
1990 Aug 24.....	CASPEC	7200	5600
1990 Aug 25.....	CASPEC	7200	5600
1990 Aug 29.....	CASPEC	7200	4300
1991 Sep 11	EMMI	10800	7300
1991 Sep 12	EMMI	10800	7300
1991 Sep 12	EMMI	10800	7300
1992 Dec 16.....	EMMI	10800	7300
1992 Dec 17.....	EMMI	10800	7300
1992 Dec 20.....	CASPEC	7200	4000
1992 Dec 21.....	CASPEC	7200	4000

calibrated, and the echelle orders were merged. This resulted in 81 different wavelength and intensity-calibrated spectra, one for each offset position of the extraction slit. These 81 spectra were arranged to create a second two-dimensional image, with wavelength as one dimension and the extraction slit offset relative to the echelle order as the other. The resulting two-dimensional image was collapsed along the wavelength direction to produce a cross-sectional profile of the spectrum, and this was used to form a weighting function. After multiplication by the weighting function, the rows of the weighted two-dimensional spectrum were averaged together to obtain the final calibrated spectrum. This method is practical because the necessary MIDAS procedures run very quickly on Sparc workstations. In addition to producing a spectrum that is easy to weight, the method has a further advantage that the backgrounds on either side of the spectrum are sampled; small biases in the initial background subtraction can be detected and corrected before the final summing of the spectral strips is performed.

Because Ray Weymann (1992, private communication) suggested to us that the spectrum of Q0059−2735 might be variable, we examined our individual spectra for evidence of variability. As we saw no evidence of obvious variability in our spectra, we have simply co-added all our individual spectra. The resulting merged spectrum was corrected to heliocentric velocities and rebinned to vacuum wavelengths.

3. MODELING THE SPECTRUM

Figure 1 gives an overview of our spectrum of Q0059−2735. We show our model of the quasar spectrum together with the data. As in our previous analysis of quasar spectra from ESO (see, e.g., Wampler, Bergeron, & Petitjean 1993), the structures, line widths, ionization conditions, and relative ion abundances of the absorbing clouds were determined by modeling the absorption lines rather than by fitting them. A MIDAS application program, CLOUD, which was written by M. Pierre, was incorporated in a MIDAS procedure that was used to generate the model. CLOUD is a derivative of ATLAS, a program written and described by Pettini et al. (1983) and later adapted to MIDAS by D'Odorico, Pettini, & Ponz (1985). CLOUD calculates model profiles using the known laboratory parameters for the transitions, convolves the results with the instrumental profile, and subtracts the absorption lines from an operator-supplied continuum level to produce an absorption model that may then be compared to the observations. The parameters can be adjusted until it is judged that a satisfactory representation of the data is obtained. This procedure does not give a "least-squares" fit to the data and therefore has the disadvantage that the fit depends on a subjective judgment and is usually not unique. In addition, many of the transitions that we see have only poorly determined atomic parameters, and these input errors are reflected in the final model. But the residuals obtained by subtracting the model from the data can be examined. This allows us to determine the dependence of the model on the input assumptions. Our method permits extensive exploration of the available parameter space. The practical limit to the number of transitions that can be simultaneously modeled is many thousands. Constraints obtained from modeling a particular transition can be applied to others within the same redshift system. For instance, as we believe that the wavelength calibration of the spectrum is accurate, we have used the velocities of unsaturated lines to determine the velocity structure of the absorbing clouds, and we used these velocities to model saturated and blended lines. Many hundreds of transitions can be used to test the input assumption against the data.

The spectrum of Q0059−2735 is very rich in absorption lines. The large number of Fe II, Cr II, Co II, Ni II, and Zn II metastable levels results in a complex absorption spectrum. Despite this complexity, groups of many lines belong to a single ionic species, and within each species, relatively few multiplets produce most of the strong absorption lines. Only four distinct velocity components (clouds) are required to explain the narrow-line spectrum. Nine additional velocity components with substantially wider profiles model the BAL flow. Thus the spectrum of Q0059−2735 is inherently simpler than the wealth of absorption features initially suggests; most of the narrow lines originate from abundant iron-peak elements; the lower lying ($\lesssim 1$ eV) metastable levels have fractional populations that are comparable to that of the ground term. Even metastable levels above 3 eV can be seen if the total column density of the ion is high enough. For each distinct velocity component we found that the relative population of the different ionic metastable levels could usually be satisfactorily represented by a single excitation temperature.

The independent parameters that must be determined in order to model the Q0059−2735 absorption spectrum are the cloud velocities, b-values, excitation temperatures, and ionic column densities. Physical parameters and the oscillator strengths, rest wavelengths, radiative lifetimes, and the statistical weights of the levels were taken from the literature. For ionic transitions from the ground terms these were mostly taken from Morton, York, & Jenkins (1988) or from Morton (1978). For the metastable terms, we used the tabulations of Fuhr, Martin, & Wiese (1988) or Kurucz & Peytremann (1975). The instrumental profile was taken to be a Gaussian with a half-width of 20 km s^{-1} for wavelengths below 6000 Å and 11 km s^{-1} for wavelengths above 6000 Å. The exact instrumental profile is not critical to our conclusions as the spectrum has many lines with greatly different optical depth that can be used to constrain the model.

A MIDAS procedure was written to generate the input tables required by CLOUD. Trial zero-volt column densities for Fe II, line b-values, redshifts, and excitation temperatures were written into the descriptors of a master table. The table for a particular transition was generated from the master table by taking into account the excitation level, relative weights, rest wavelengths, and multiplet number. The procedure generates the required input table by calculating from the cloud

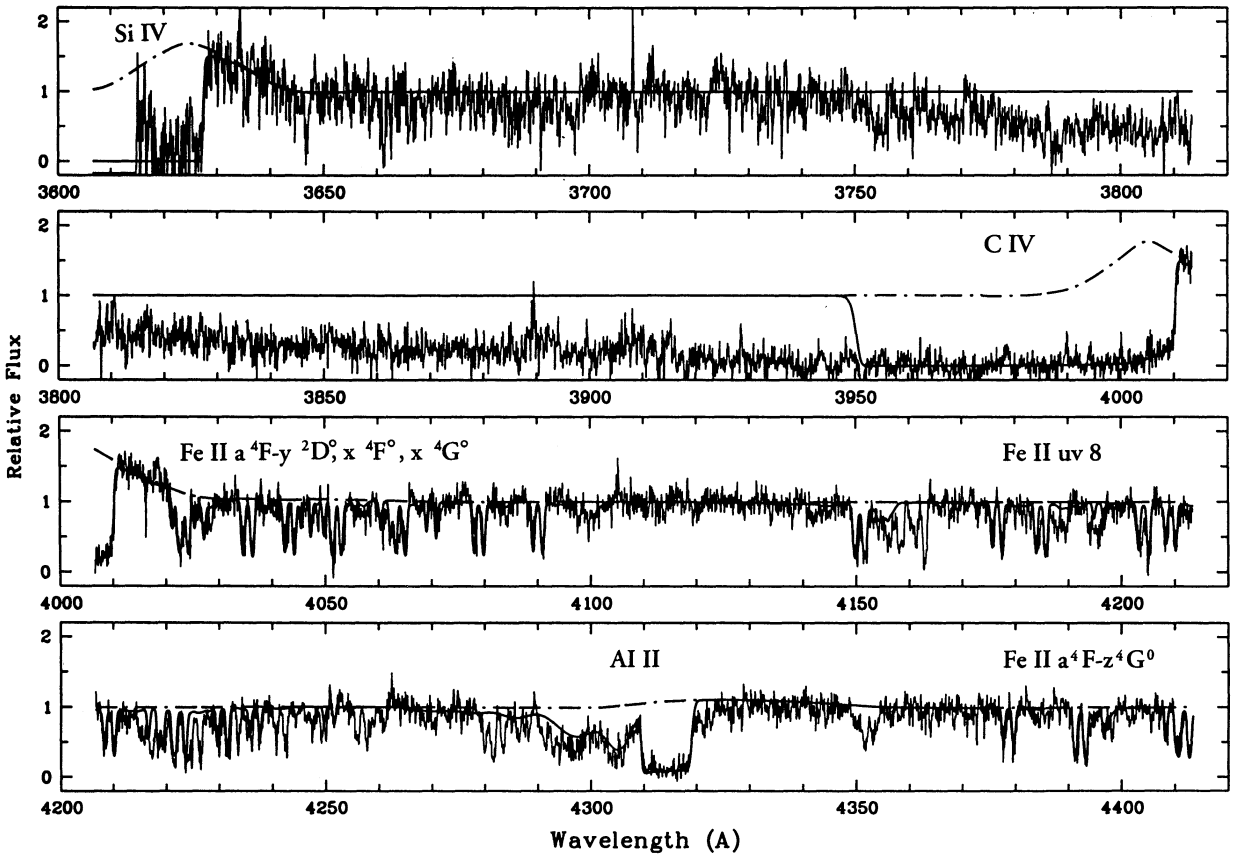

FIG. 1a

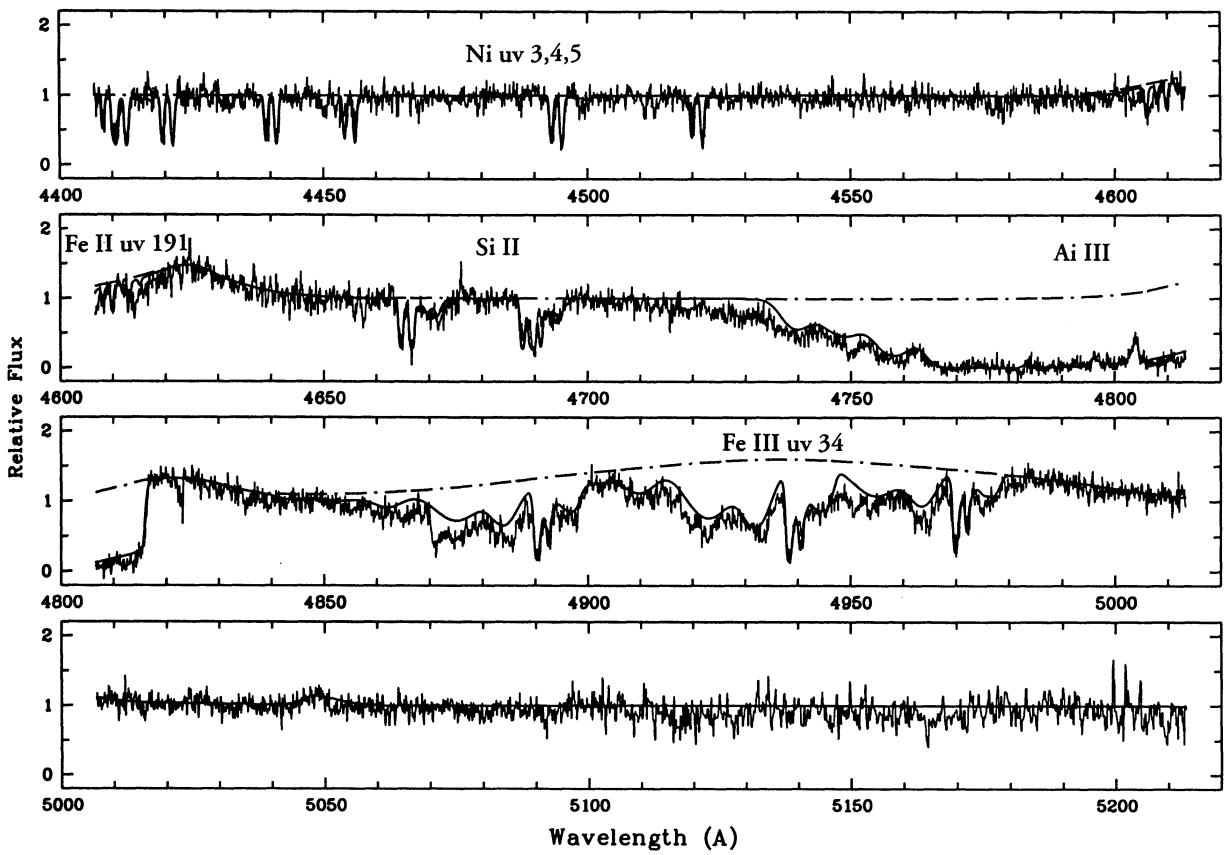

FIG. 1b

FIG. 1.—Overview of the high-resolution spectrum of Q0059−2735. *Thin continuous line*, quasar spectrum; *heavy solid line*, our absorption model; *dot-dashed line*, our adopted continuum.

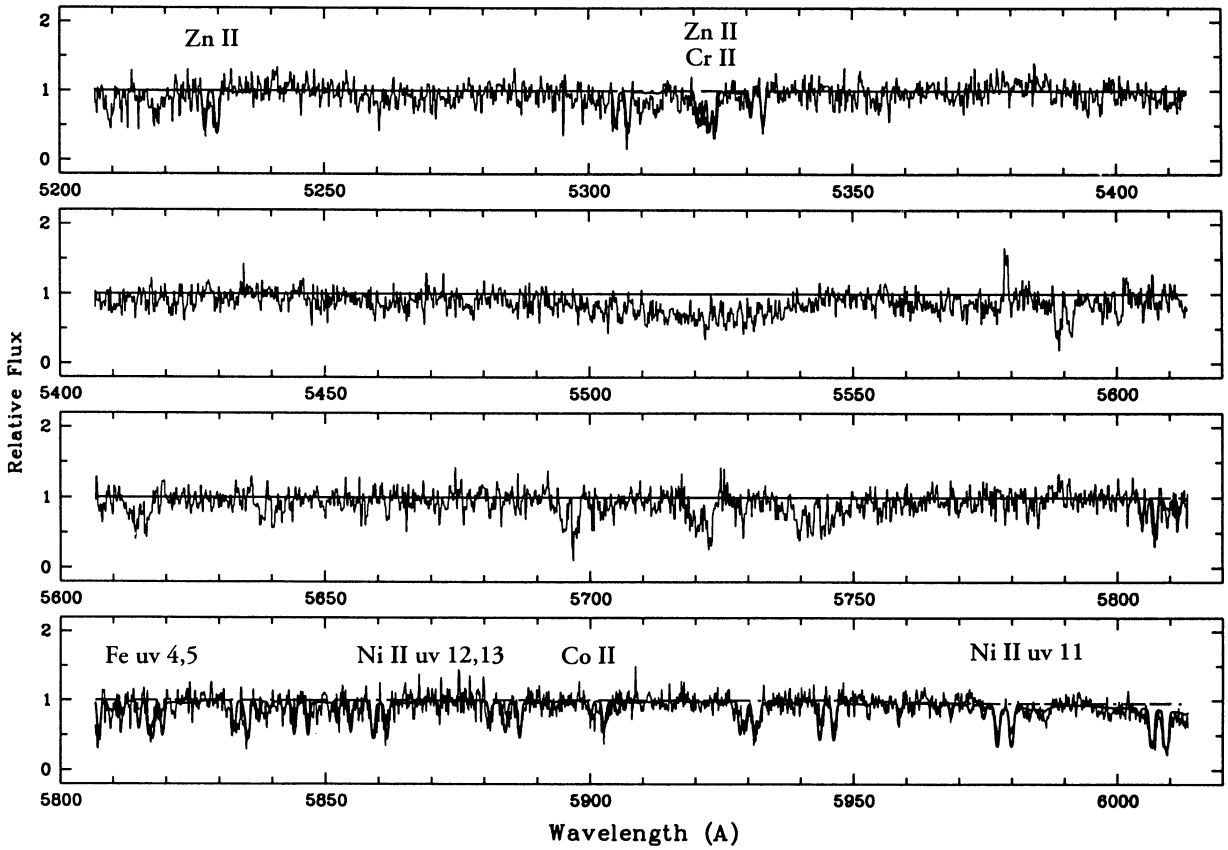

FIG. 1c

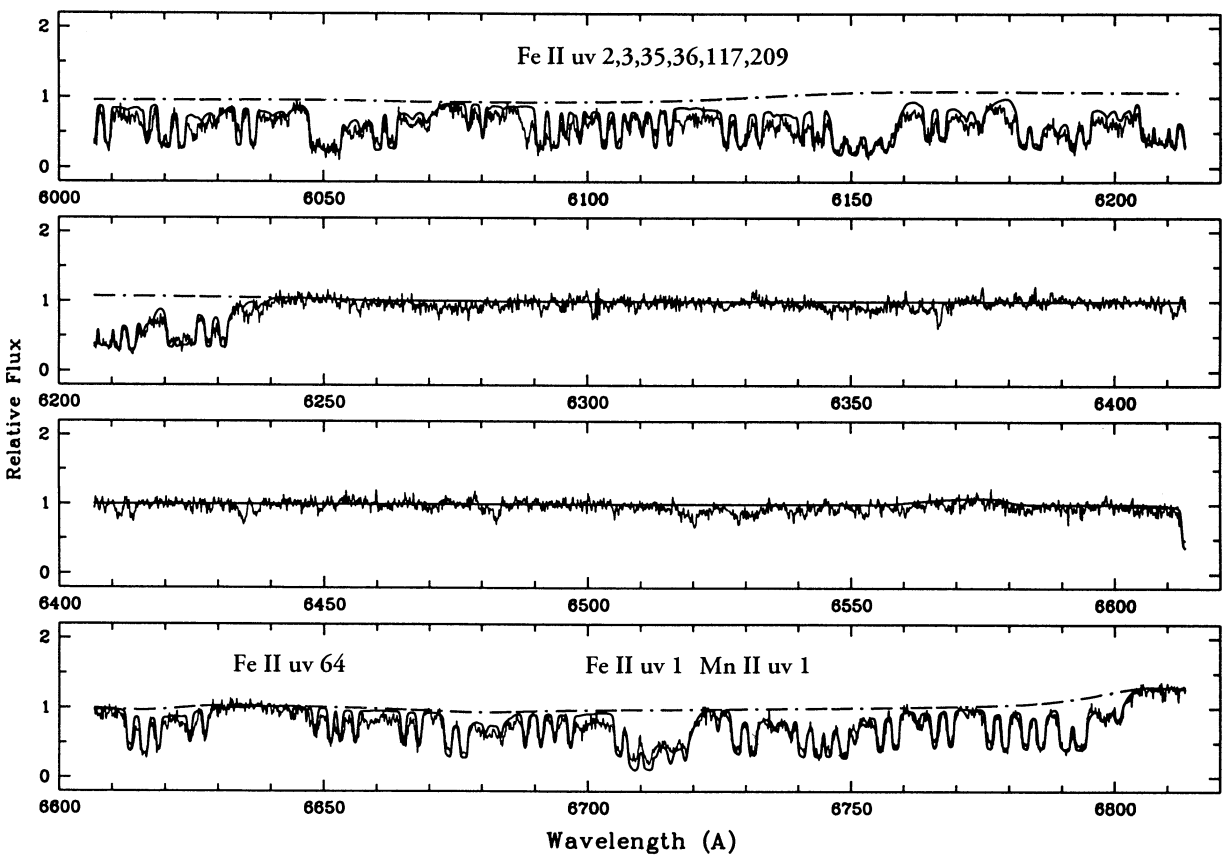

FIG. 1d

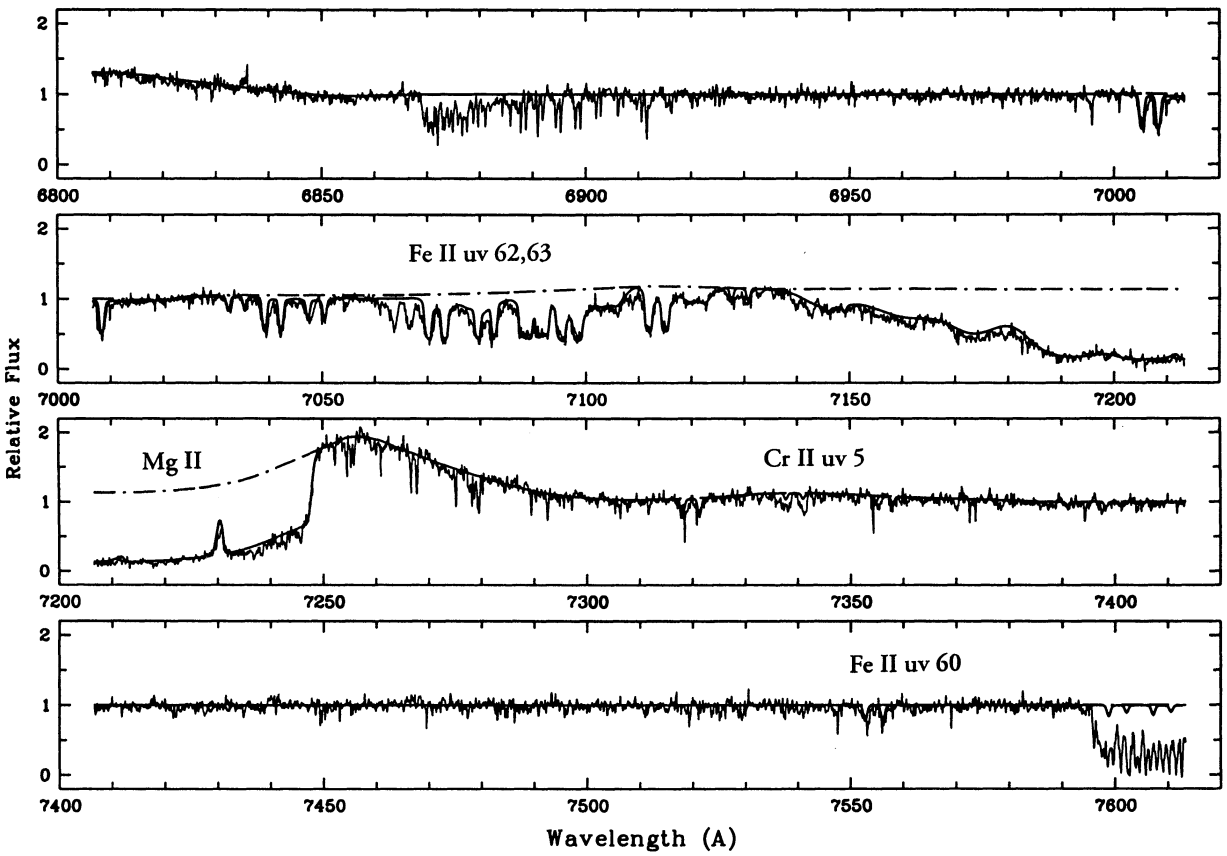

FIG. 1*e*

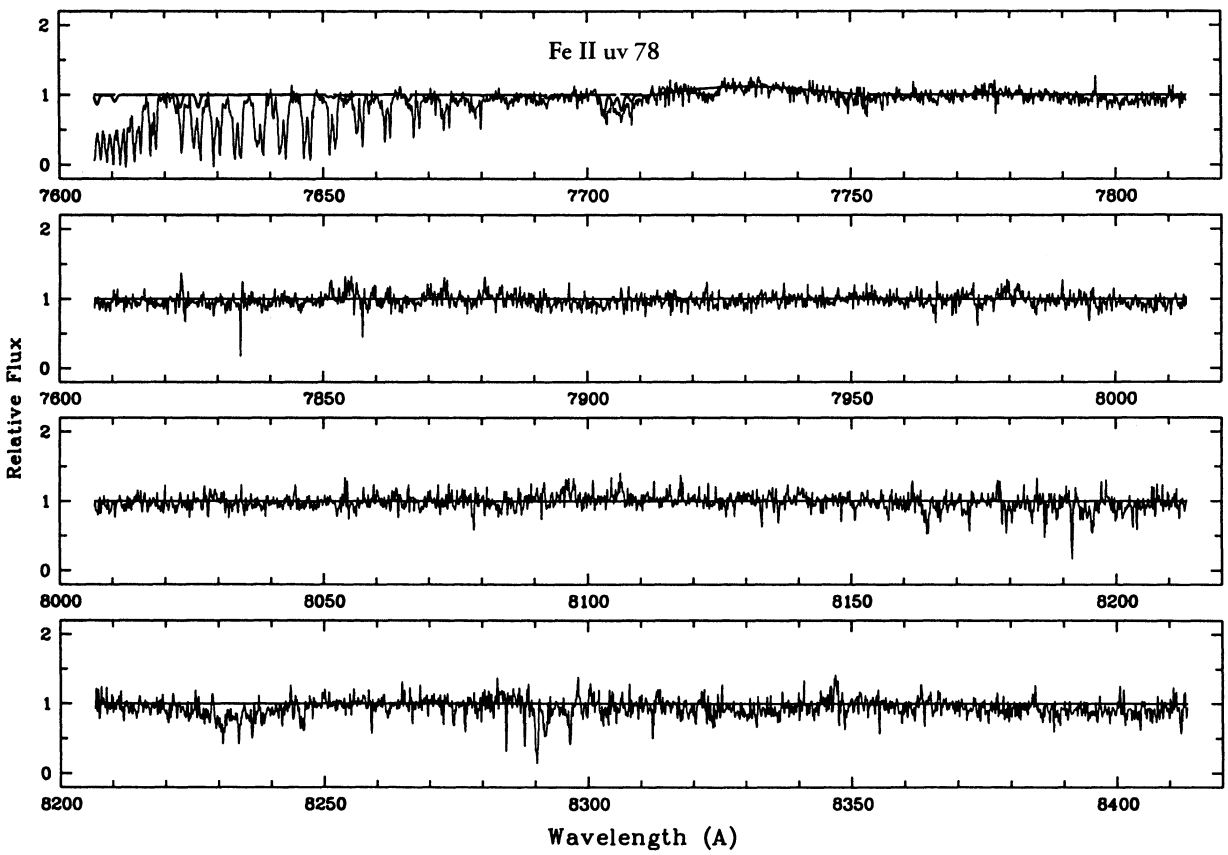

FIG. 1*f*

TABLE 2

PHYSICAL PARAMETERS FOR THE CLOUD MODELS

Cloud No.	Redshift (z)	Velocity (km s^{-1})	b-Value (km s^{-1})	Excitation Temperature (10^4 K)	Relative Column Density
			NAL		
1	1.58386	0	30	0.4	0.01
2	1.58275	130	30	0.4	0.0063
3	1.58115	315	17	0.5	1.0
4	1.58000	450	17	0.7	0.5
			BAL		
5	1.5839	−5	80	0.9	0.014
6	1.5828	+125	100	0.9	0.02
7	1.5812	310	80	0.9	0.025
8	1.5801	435	50	1.1	0.013
9	1.5768	820	200	3.0	0.0025
10	1.5721	1365	350	4.0	0.0025
11	1.5652	2140	250	6.0	0.0005
12	1.5603	2740	350	5.0	0.00038
13	1.5554	3325	220	5.0	0.00016

redshifts the observed vacuum wavelengths of the transitions and obtaining the column densities by assuming that within each term the level populations are proportional to the statistical weights of the level multiplied by the excitation factor. Within each term the assumption that the population is distributed by the ratio of the statistical weights, works well. Because the derived excitation temperatures are $\gtrsim 10^4$ K, it proved unnecessary to complicate the modeling by taking into account the different excitation levels within a term. In the absence of detailed calculations of excitation and de-excitation rates for individual levels that can be tested against the observations, there is no compelling reason, at present, to abandon the simplification that the levels within a term are populated by their statistical weights. The relative term populations were calculated using the excitation temperatures derived for each velocity system.

Our models are almost certainly not correct in detail; a few of the observed features are, in fact, poorly matched by the final models. These discrepancies are usually in the sense that the strength of an absorption feature is underestimated. At the present time we are uncertain whether these discrepancies between the model and the observed spectrum are caused by our failure to take into account all relevant transitions, or by errors in the input physical parameters of the lines, or by errors in the observational data. Despite these drawbacks, our models are sufficiently constrained by the complexity of the Q0059−2735 spectrum to permit useful conclusions to be drawn about the nature of this BAL quasar.

Table 2 gives the cloud parameters—the excitation temperatures, the b-values, and the velocities—for the NAL and BAL models. The tabulated velocities are relative to a standard of rest defined by the highest velocity NAL cloud, and the sign was chosen so that motion toward the observer (outflow) was treated as a positive velocity. In Table 3 we give the derived column densities for the various ions. In the following subsections we discuss in detail the construction of the NAL and BAL models, using the constraints placed on the absorption models by the data.

3.1. *The NAL Clouds*

Substantial population in those metastable levels which have excitation potentials up to a few eV is needed to explain the spectrum. We have estimated the relative population of the excited metastable levels by predicting their population from a set of models using different excitation temperatures. For each trial excitation temperature, the cloud b-values were adjusted to find the most suitable value for each adopted temperature. Because the observed multiplets have a wide range of gf-values, it is possible to obtain a fairly good estimate of the effective excitation temperatures and b-values.

The most prominent narrow lines are strongly saturated; this is evident both from the observation that Fe II multiplets,

TABLE 3

IONIC COLUMN DENSITIES

A. COLUMN DENSITIES FOR NAL CLOUD NO. 3[a]

	Si II	Cr II	Mn II	Fe II	Fe III[b]	Co II[b]	Ni II	Zn II
Ground state.....	1.4×10^{17}	1.6×10^{14}	4.7×10^{13}	1.2×10^{16}	8.0×10^{17}	7.0×10^{13}	3.0×10^{15}	1.0×10^{14}
All states	1.4×10^{17}	1.9×10^{14}	5.2×10^{13}	2.1×10^{16}	8.0×10^{17}	1.1×10^{14}	3.3×10^{15}	1.0×10^{14}

B. COLUMN DENSITIES FOR BAL CLOUD NO. 5[a]

	Mg II	Si II	Al II	Fe II	Fe III[b]	Al III	Si IV	C IV
All states	2.2×10^{15}	2.0×10^{15}	2.2×10^{14}	5.0×10^{14}	4.0×10^{16}	4.8×10^{15}	4.4×10^{17}	2.4×10^{18}

[a] Use the parameters given in Table 2 to scale the column densities for other clouds.
[b] Calculated from excited state; see the text.

say, UV4 or UV5 have comparable strengths to UV1 or UV2 despite the fact that the oscillator strengths for UV4 and UV5 are only 1/100 of those for UV1 and UV2 and from the fact the line profile of many of the narrow lines have the square, flat-bottomed profiles characteristic of saturated absorption features. Moreover, the saturated NALS have substantial residual intensity in the line bottoms; they do not reach zero intensity. Apparently, there are nonocculted radiation sources that fill in the line bottoms. The fractional residual intensity at the bottom of the saturated lines ranges from ~25% at 4000 Å to ~50% at 7000 Å. If the continuum that is not covered by the narrow lines is due to a thermal source, then a simple fit to the residual intensity at 4000 Å and at 7000 Å gives a temperature of $T \approx 17{,}000$ K if the Q0059−2735 continuum spectral index is 0. This drops to $T \approx 13{,}000$ K if the continuum spectral index is 1.0. Because we do not have accurate photometry of the relative continuum levels of Q0059−2735 in the blue and red, we have used trial spectral indices that cover the normal span seen in QSO spectra. Other continuum sources are possible, but the data are not yet good enough to test more complicated continuum sources.

The strong Fe II lines near Mg II have substantially more residual intensity in the line centers than does the Mg II λ2800 BAL absorption. For instance, the Fe II multiplets UV62 and UV64 at ~7100 Å lie only slightly to the blue of Mg II at ~7200 Å, yet the saturated Fe II line bottoms have a much higher residual intensity than does the Mg II BAL absorption (see Fig. 1). The conclusion must be that the NAL clouds cover a smaller fraction of the Q0059−2735 nuclear continuum source than does the Mg II BAL absorption. In our model for the narrow-line absorption, we have included a nonocculted radiation source for the narrow lines, but we have assumed that any BAL absorption associated with the NALs, like that of the Mg II BAL absorption, covers the *entire* continuum region. This BAL absorption component has the effect of depressing the continuum level against which the narrow lines are formed. While it is clear that the continuum source underlying the Fe II lines rises steeply toward the red, the source of this residual intensity in the bottom of the NALs is still uncertain. One possibility is that it is a comparatively low temperature thermal continuum. A second possibility is that some of the underlying "continuum" is Fe II emission, which also is strong in quasar spectra at rest wavelengths of 1900–3800 Å. But any Fe II emission must be only a minor contributor to the residual intensity in the Fe II UV62 and UV64 multiplets, since there is little evidence for strong Fe II emission either in the Mg II BAL absorption trough, or between the individual Fe II absorption components.

Figure 2 shows that the narrow-line iron spectrum shows interesting patterns in the populations of the metastable levels. Transitions from multiplets UV62, UV63, and UV64 that come from the Fe II a^4D (1 eV) term and transitions from multiplets UV35 and UV36 from the Fe II a^4F term (0.3 eV) are comparable in strength with transitions from UV1, which

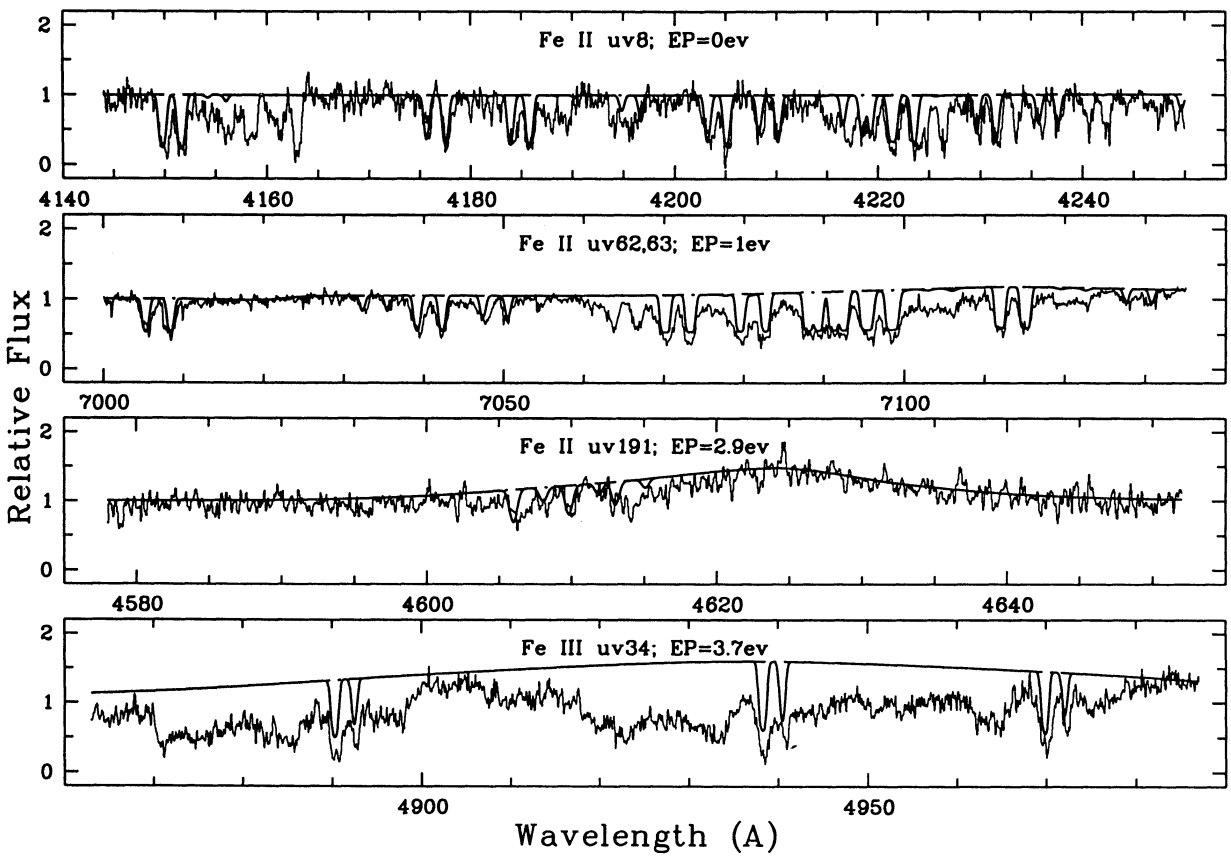

FIG. 2.—NAL absorptions originating from terms with increasing excitation potential. Note that the relative strengths of the strong pair of lines (clouds 3 and 4 in Table 2) reverse as the excitation potential of the lower term increases. For ground terms, cloud 3 is twice as strong as cloud 4; for Fe III (EP = 3.7 eV), cloud 4 is 6 times as strong as cloud 3.

originate from the Fe II a^6D ground term. A comparison of the strength of Fe II UV78 lines with those from UV1 shows that the UV78 lines from the Fe II a^4P (1.7 eV) term are present, but are much weaker than the lines from the Fe II a^6D ground term. The next higher set of levels in the ^4P series is at 2.7 eV. But the multiplet lines from Fe II b^4P are blended both with lines from the ground-term multiplets UV1 and UV2 and with lines from multiplet UV64. The strength of the transitions from Fe II b^4P is therefore hard to determine with certainty, but the population of Fe II b^4P is certainly much less than the population of the ground term.

Hazard et al. (1987) noted that lines from multiplet UV91, which originates from the 2.9 eV a^6S level of Fe II, were present in their spectra of Q0059−2735. We agree with this identification. The multiplet UV191 spectral region is shown in Figure 2. The observed emission feature at this wavelength seems to be in good agreement with the predicted wavelength for multiplet UV191 emission if we scale the Mg II emission line to the position of UV191. In both cases the peak of the emission line lies $\sim$900 km s^{-1} to the red of the absorption lines. The excitation temperatures given in Table 2 for the 310 km s^{-1} and 450 km s^{-1} clouds are largely determined by the level populations in the a^6S term. As Figure 3 shows, in multiplet UV191 the 450 km s^{-1} cloud absorption is about twice as strong as that of the 310 km s^{-1} cloud, but in the spectrum of the Fe II ground term the 310 km s^{-1} cloud absorption is stronger than that of the 450 km s^{-1} cloud. The spectrum of Fe II multiplets UV62 and UV63, which originate from the 1 eV a^4D level, shows an intermediate situation: the 450 km s^{-1} and 310 km s^{-1} clouds have comparable absorption strengths. These facts show that the excitation temperature of the 450 km s^{-1} cloud is higher than that of the 310 km s^{-1} cloud. In fact, the excitation temperatures for the 450 km s^{-1} and 310 km s^{-1} clouds seem to be reasonably well established by the Fe II data. An examination of the spectra of Ni II and Cr II shows that a similar excitation temperature to that found for Fe II also gives good fits to the spectra originating from the metastable levels of these ions.

The excitation temperatures of the two lower velocity NAL clouds (at 0 km s^{-1} and 130 km s^{-1}) are not as well determined. The two components are clearly seen only in strong Fe II transitions that originate from terms that have excitation potentials less than $\sim$1.5 eV. But the excitation temperature cannot be very much more than that for the two strong, higher velocity, clouds or they would be seen in the multiplet UV78; nor can it be much less or they would not be visible in the spectrum of Fe II multiplets UV62 and UV63.

The determination of the ionic column densities require, in addition to the excitation temperature, an estimate of the absorption-line b-values. Because many of the narrow lines are saturated, this requires a comparison of strong and weak transitions from the same lower level. The Fe II transitions from the ground term proved to be best for this comparison. We have calculated models with b-values ranging from 8 to 35 km s^{-1}. Accessible within our spectral bandpass are transitions from the Fe II a^6D ground term with oscillator strengths ranging from 0.3 to 2×10^{-4}. Particularly important are the Fe II multiplets UV4 and UV5, for which the f-values are $\sim 3 \times 10^{-3}$, but which are fairly strong and are mostly free from blending with other lines. The multiplet lines, UV60, UV62, and UV63 originating from the 1 eV a^4D level provided a check on the b-values determined from the ground-term multiplets. The chosen value, $b = 17$ km s^{-1}, gives acceptable fits to the data, but again, as was the case for the excitation temperature, the b-values for the two lower velocity NAL clouds are poorly determined. Substantial improvement in all these parameters may be obtained when better radiative and collisional models as well as higher signal-to-noise spectra become available.

Figure 3 shows several spectral regions where relatively unblended absorptions from Cr^+, Co^+, Ni^+, and Zn^+ are found. Numerous lines from each of these ionic species are available for comparison with the model. However, for Co^+ the column density was determined by fitting multiplet UV9. This multiplet originates from the a^5F term of Co II, which is a metastable level with an excitation potential of $\sim$0.5 eV. We therefore have to trust our excitation model to convert the derived column density for this single term into a total column density for the ion. We would like to check the determination of our column density by fitting other multiplets, and in particular, with transitions from the ground term, but we have found no unblended Co II in low-noise spectral regions. The lack of other accessible Co II transitions is consistent with the strength of the UV9 transitions and our excitation model. The Mn II absorption lines from the ground term are located in the region of strong Fe II absorption near 6700 Å. Nevertheless, as Figure 3 shows, it seems possible to estimate the strength of the Mn II NAL absorption from those lines that are relatively free of Fe II contamination.

In Q0059−2735 both the Zn II and Cr II lines are strong (see also Table 3). The Cr II/Zn II ratio is 1.9; this value is approximately the median ratio found by Pettini et al. (1994) in a survey of 17 damped Lyα systems. The implied depletion of Cr with respect to Zn is [Cr/Zn] ≈ -0.9. Thus we find that the line-absorption region of Q0059−2735 is moderately dusty, with a gas-to-dust ratio similar to that found by Pettini et al. (1994) for isolated damped Lyα systems at $z \sim 2.5$.

Hazard et al. (1987) tentatively identified the presence of N I lines from UV9 at $\lambda_{obs} = 4493$ Å. We do not confirm this identification. Some lines are present near the expected wavelengths, but the wavelength discrepancy is too great, and the pattern of the absorptions does not agree with their identification as the N I UV9 transitions. Instead, we have identified the transitions as lines from the ground-term Ni II UV5 multiplet.

3.2. *The BAL Flow*

We have constructed our BAL model by convolving Gaussian absorption components with velocities, column densities, and b-values chosen to match the observed features in the BAL flow. In order to obtain satisfactory model fits to the absorption lines it is necessary to accurately locate the continuum level. This is difficult to do in regions of strong absorption. The continua we chose are ad hoc, but plausible, representations of the actual continuum level. An inspection of Figure 4 shows that the red transition from the continuum level to deep Mg II absorption is abrupt, that there is residual flux in the bottom of the absorption trough, and that there is a sharp, narrow reversal in the BAL trough. The probable explanation for the general luminosity in the bottom of the Mg II absorption is that, while the Mg II absorption cloud covers *all* the central continua sources, it is not covering the Mg II broad emission line (BEL) region. If the Mg II emission line is reflected about the apparent emission peak at $\lambda_{vac} = 7257$ Å, the blue half of the Mg II BEL extends to $\sim$7220 Å. This is the wavelength of the start of the rise in residual intensity in the red part of the Mg II BAL absorption (see Figs. 1*e* and 4). Furthermore, the rate of the observed rise in the Mg II residual is within $\sim$10%

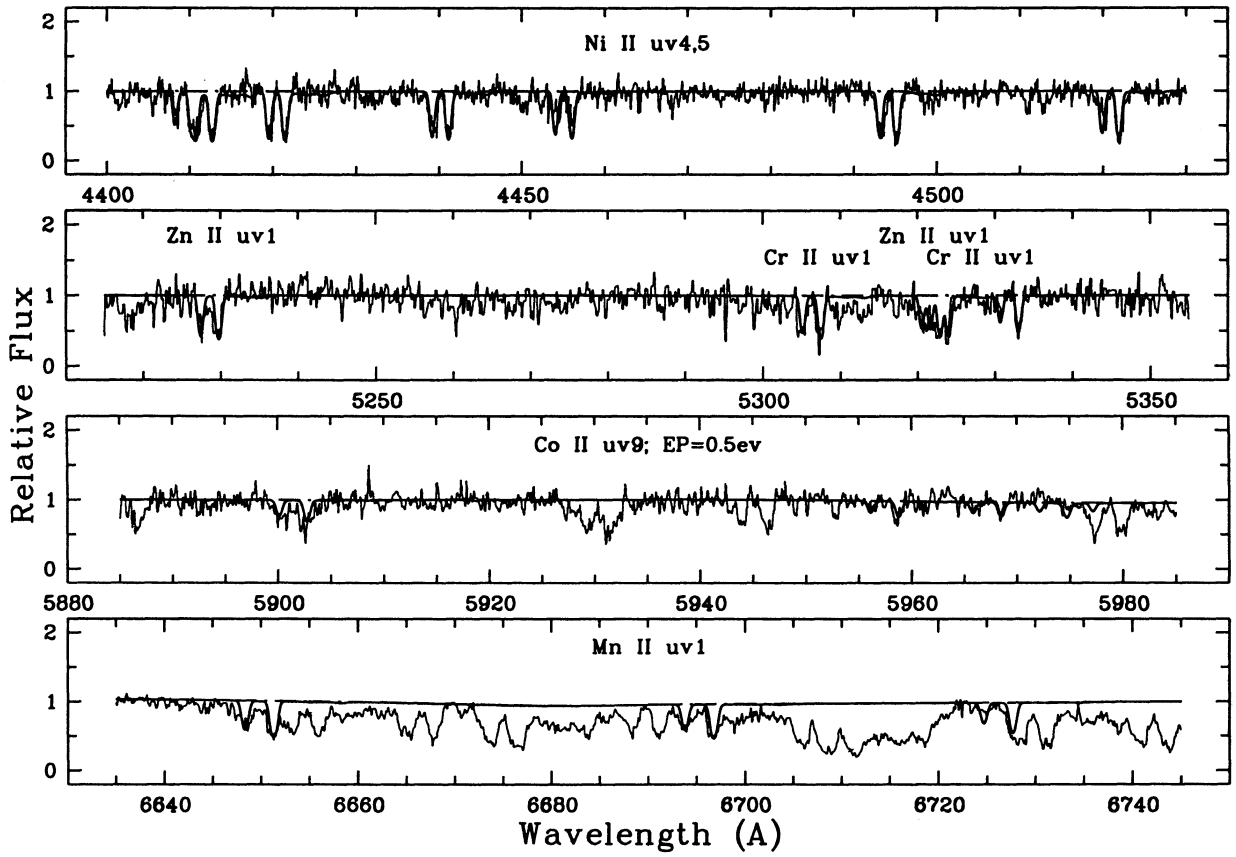

FIG. 3.—Transitions that establish the column densities for Cr II, Zn II, Co II, Ni II, and Mn II

of the rate of rise expected if the residual intensity were due to a blue Mg II emission wing that is symmetrical with the red wing. Small discrepancies may be due to slight asymmetries in the line profile, or to comparatively weak Fe II emission. Similarly, the residual intensities seen in the bottoms of the Al II and Al III BAL absorptions are reasonably explained by the failure of the ionized Al BAL flows in covering the corresponding aluminum emission-line regions.

An important consequence of this profile fitting is that the small drop in intensity between the Mg II emission peak and the onset of the strong BAL absorption is due to a true decrease in the intensity of Mg II emission, rather than due to weak red absorption wings in the Mg II BAL flow. Thus, the emission peak of Mg II lies ~ 9 Å to the red of the onset of the BAL absorption. It is unclear what Mg II wavelength should correspond to the peak of the Mg II BEL. But if the two Mg II BEL doublet lines have similar intensity, the BEL peak would then lie 22 Å (~ 900 km s^{-1}) to the red of the highest redshift of the Mg II narrow-line system. And if the Mg II emission-line peak represents center-of-mass motion of Q0059−2735, then the NAL cloud with the lowest outflow would be moving toward the observer at ~ 900 km s^{-1} with respect to the quasar center of mass. This velocity is similar to the likely difference in velocity between the Mg II and C IV emission lines (see below).

The five highest velocity components of the BAL flow can be clearly seen as absorption dips in the higher velocity (unsaturated) parts of the Mg II BAL flow (see Fig. 4 and Table 2). These ripples are seen in the Al III BAL absorption, and the stronger ones also appear in the Al II BAL absorption. It is notable that these five components are approximately spaced apart by the Mg II doublet separation. This modulation in the Mg II BAL flow may represent the beginnings of organization in the Q0059−2735 BAL gas flow. The possibility of organization in BAL flows was first suggested by Scargle, Caroff, & Nordlinger (1970) and Scargle (1973) to explain absorption-absorption line locking in QSO spectra. The line-locked absorptions seen in the quasar Q2116−358 at the positions of C IV, Si IV, and N V may represent a later stage in the development of such flows (Wampler et al. 1993).

The low-velocity BAL flow is saturated in the lines of Al II, and Mg II. Because the Fe II BAL absorption is spread over so many multiplet transitions, it is unsaturated, and one can estimate the structure and strength of the Fe II BAL flow. As illustrated in Figures 1 and 4, weak BAL absorption is needed to depress the rise to the continuum level that would normally occur between the saturated NAL components. These low-velocity BAL components can also be seen in the weak Si II λ1808 transitions. In our first attempt to model the low-velocity part of the BAL flow we used two clouds, one with a central velocity near 0 km s^{-1} and a b-value of 100 km s^{-1}, the other with a central velocity near 200 km s^{-1} and a b-value of 230 km s^{-1}. The combination of these two components produced a wedge-shaped profile that could be made to suitably match the observed Si II and Fe II profiles while at the same time producing the saturated components for Mg II, Al II, and Al III. However, while these two clouds could be adjusted to fit Si II and Fe II rather well, the wings of the model were too

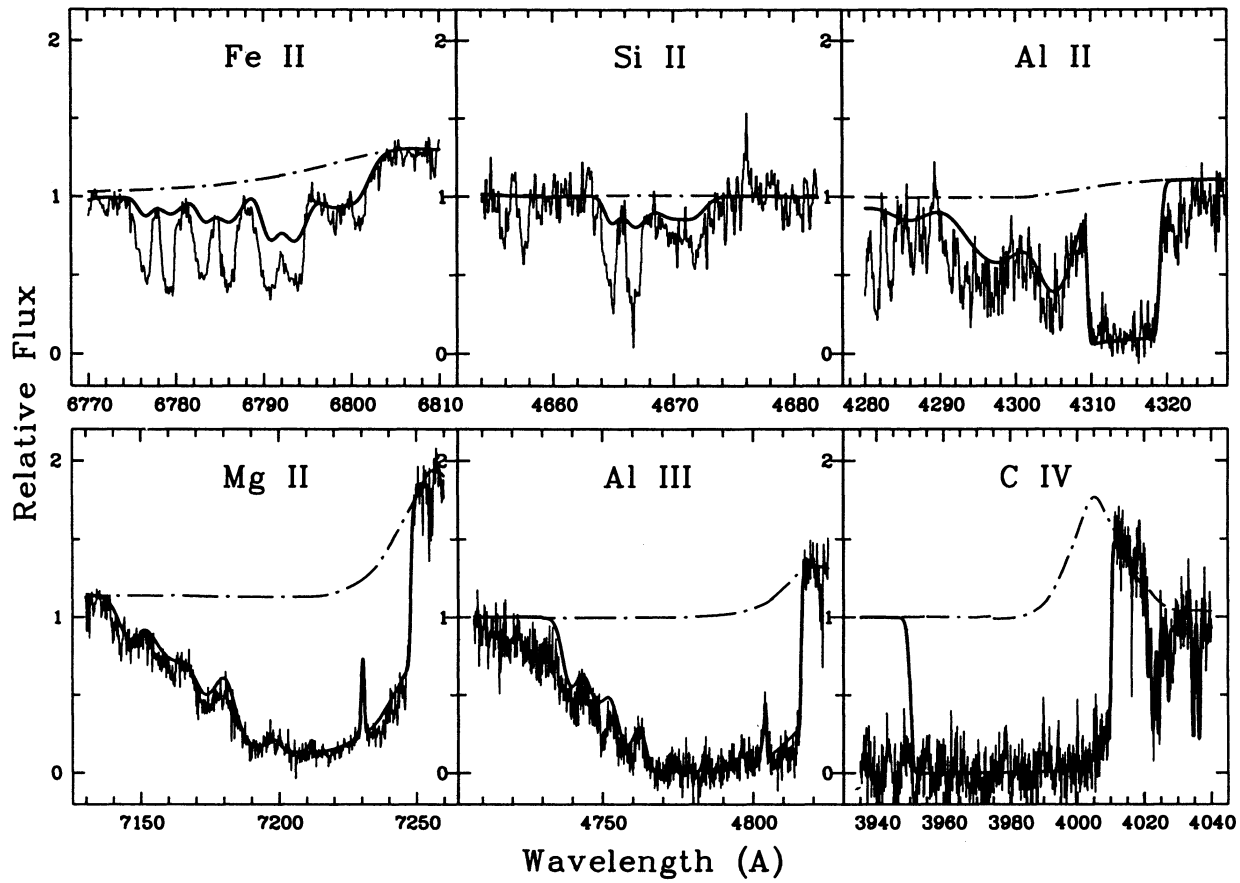

FIG. 4.—BAL lines in Q0059−2735. The continuous line is the model; the adopted continuum is the dot-dashed line. The model is the same for all components. Only the total column density is different for the different ions.

shallow to fit the steep rise seen in the red wing of the Mg II and Al III profiles, nor would the profile fit the two steep edges of the deep, low-velocity Al II BAL absorption.

The clue to obtaining a more satisfactory fit was provided by noting that the velocities required for these strongest components were similar to the velocities of the NAL clouds. We therefore replaced our first ad hoc two-component model with four cloud components which has velocities chosen to be similar to those of the NAL clouds. This type of cloud structure could represent modest BAL components associated with a transition between the BAL flow and the four NAL clouds. The required four BAL clouds were found to require column densities, *b*-values, and excitation temperatures that are intermediate between those determined for the NAL clouds and the higher velocity BAL clouds.

The choice of the BAL absorption profile is critical to the determination of the relative ionic column densities in the Q0059−2735 BAL flow. Only the strongest BAL components are clearly seen in the Fe II absorption, and it is just these components that are saturated in the Mg II and Al III BAL flow. But once the cloud velocities and *b*-values had been chosen, the requirement that the wings of the clouds match the location and slope of the observed absorption edges (which are quite steep) gives a tight constraint on the BAL column densities for the ions that have saturated BAL flows.

The observed weak, narrow reversal seen in the Mg II BAL absorption at $\lambda_{vac} = 7230$ Å appears to be due to a gap between the NALs of the Mg II doublet system. In fact, the steep red edge of the narrow Mg II emission reversal is defined by the blue wing of the 435 km s^{-1} BAL. The blue wing of this reversal is not as steep as the red wing; it is produced by the 820 km s^{-1} BAL cloud, which has a much higher *b*-value than does the 435 km s^{-1} BAL. A similar reversal to that found in the Mg II BAL absorption is seen in the bottom of the Al III BAL trough. When the column densities and wavelengths of the Mg II BAL absorption model are scaled to fit the low-velocity Al III BAL feature, it was found that the higher velocity BAL clouds, which are not saturated, also fit the Al III BAL profile. *The relative strengths and velocities of the modeled* Fe II, Si II, Mg II, Al II, *and* Al III *BAL absorption components are identical to within the precision of the data.* The models for Si IV and C IV are not as well constrained as those for the lower ionization ions because the saturation of these higher ionization BAL lines are much stronger, but scaling up the low-ionization model column densities until the model fits the Si IV and C IV absorptions gives ionic column densities that are in agreement with our ionization model for Q0059−2735 (see § 4.2).

Lowering the *b*-value of the four lowest velocity BAL clouds to less than 80 km s^{-1} gives the very steep transitions that are needed to fit the steep edges of the low-velocity BAL flow. We also found that the nine-cloud BAL model led to derived ionization parameters that were similar for the BAL and the NAL clouds, while when we used the seven-cloud model with higher

b-values for the low-velocity clouds, the ionization parameter was an order of magnitude higher for the NAL clouds than it was for the BAL clouds. This is because the seven-cloud BAL model had less line saturation than the nine-cloud model. This resulted in a lower Al^{++}/Al^{+} ratio for the seven-cloud model than for the nine-cloud model. If the ionization parameter *is* lower for the BAL clouds than for the NAL clouds then either the NAL clouds have lower density than the BAL clouds or they are closer to Q0059−2735 nucleus than the BAL clouds. Because we find that the low-velocity BAL clouds have velocities that are very similar to those of the NAL clouds, we think that they are formed in approximately the same place and that any differences in BAL and NAL ionization parameters should be in the opposite sense from that required for the seven-cloud model.

Decreasing the tabulated column density of the nine-cloud model by a factor of 3 leads to unacceptable residual intensity in the bottoms of the low-ionization lines, while increasing the column density by a factor of 3 would result in absorption that would spread beyond the BAL widths seen in the spectrum. However, if our model is inappropriate; if the wings of the components were, for instance, truncated rather than exponential decreasing, we could somewhat increase the column densities of the low-velocity components in the Mg II, Al II, Al III, and C IV BAL flows and still fit the observed profiles. But we cannot substantially modify the structure of the low-velocity BAL clouds without compromising the fit to the Fe II lines. Consequently, we have adopted the nine-cloud model, and we believe that we have determined the relative column densities of Fe II, Si II, Mg II, Al II, and Al III in the BAL flow to within a factor of 2.

The Fe III triplet UV34 was used to determine the excitation temperature of the Fe III BAL clouds. The three Fe III UV34 lines show strong overlapping BAL absorption, but unlike the case for Al III, the lowest velocity BAL absorption is rather weak compared to the higher velocity clouds. The excitation potential for the level producing UV34 triplet is 3.7 eV, and it is almost certain that the different appearance of the Fe III BAL absorption from that of Al III is caused by the fact that the Al III BAL absorption comes from the ground term while the Fe III BAL absorption is from a highly excited state. We were able to estimate the temperatures for the nine BAL velocity components by first determining the temperatures of the four lowest velocity BAL clouds from a comparison of the strength of these absorptions in the ground term of the Fe II spectrum with their strength in the Fe II UV62, UV63, and UV191 multiplets. Multiplet UV191 sets an upper limit for the excitation temperature, while the other two set lower limits. Because we have found that the distribution of Al^{+2} ions in the different velocity components is the same as the distribution of singly ionized ions, the ionization and chemical structure of the Q0059−2735 BAL flow seems to be independent of cloud velocity. It therefore seems probable that the distribution of column densities in the different velocity systems is the same for the Fe^{+2} ions as it is for Al^{+2} and the singly ionized ions. Following the determination of the excitation temperature of the low-velocity Fe III BAL clouds, it is then a simple matter to determine the excitation temperature of the higher velocity Fe III BAL clouds because one can use the Al^{+2} population ratios to estimate the ground-state Fe^{+2} column density in each cloud.

Table 2 shows that the excitation temperatures determined in this fashion show a steady increase with velocity. Figure 5

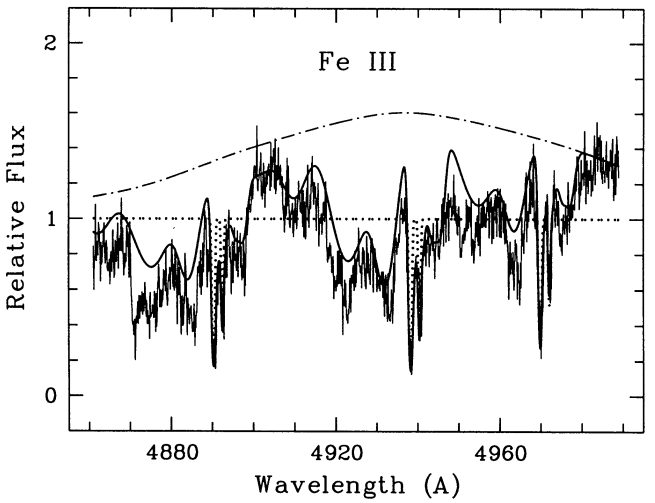

FIG. 5.—Fe III UV34 region showing the absorption profile resulting from the combination of the BAL and NAL components. The dotted line shows the saturated NAL spectrum of Fe III with a flat underlying continuum. This NAL spectrum must absorb *all* the assumed BEL spectrum, here indicated by a dot-dashed line.

shows the fit of the Fe III BAL model to the data. For Fe III the determination of the background continuum level is critical to the details of the fit, as the three strong lines are spaced apart in such a way that overlapping BAL components complicate the fit. To add to the complication, the Fe III UV34 lines lie at the same wavelength as the C III] λ1909 broad emission feature. If the redshift of the peak of the C III] λ1909 emission line is the same as that of the Mg II BEL, then the peak emission should be at approximately 4947 Å. This is just the location of the redshifted Fe III λ1910 line. The likely presence of C III] emission is signaled by an apparent red wing that lies in the observed interval 4980–5020 Å (see Figs. 1*b* and 5). In an attempt to estimate the likely C III] emission profile, we shifted the Mg II emission line to the expected position of C III] and then scaled the line strength to fit the apparent C III] emission wing that lies clear of the red Fe III absorption. This profile, slightly smoothed, is shown as a dot-dashed line in Figure 5.

It became clear to us, after many attempts to fit the Fe III UV34 lines, that, unlike the case for Mg II, Al II, and Al III, the Fe III absorption lines *completely* cover the C III] λ1909 emission feature. This is an important geometrical constraint on models for the line-forming region of Q0059−2735. An inspection of Figures 4 (at Si II), 5, and 2 (*top*) shows that the residual intensities of the narrow lines is ~0.3 (Si II at 4665 Å), ~0.3 (Fe III at 4940 Å), and ~0.4 (Zn II at 5230 Å). Thus the Fe III NALs have the same residual intensity as other, nearby, metal lines despite the fact that the Fe III NALs are superimposed on C III] λ1909 emission. Because the excess radiation at $\lambda\lambda_{obs}$ = 4900 and 4980 Å exceeds 1.2 times the continuum level outside the C III] emission-line region, and this excess, which would easily be seen, is not reflected by an increase in the residual intensity in the bottoms of the Fe III NALs, the Fe III NAL region must cover the C III] emission line region. The Fe III NALs are saturated; the dotted line in Figure 5 shows the result obtained when the residual intensity in the Fe III NALs is set to a value intermediate between that seen for Si II and Zn II. There is no margin for the required background radiation from C III] emission.

The above statements are independent of the exact shape

and strength of the C III] BEL. They require only that the strength of the C III] BEL at the peak intensity as seen by the NAL region increase the local continuum level by at least 10% of the continuum value. This requirement is probably met since the rise we identify as the wing of C III] λ1909 already rises to 20% of the continuum local continuum level and the other emission lines in Q0059−2735 are strong. Our model fits show also that the Fe^{+2} BAL triplet are not saturated and they therefore cannot completely extinguish the C III] emission line. The optical depth of the Fe^{+2} BAL must be less than 0.5. The Fe^{+2} BAL region is probably not smaller than the Fe^{+2} NAL region, but because the BAL absorption is not optically thick, it is possible to reproduce the spectrum modulation using selected combinations of absorption- and emission-line strengths. The model shown in Figure 5 assumed that both the BAL and NAL absorbing regions covered the C III] BEL region.

Other lines are present in this spectral region. For instance, the Si III intercombination line at 1895 Å is blended with the Fe III line at 1895.456 Å. But the other two Fe III lines at 1914.056 Å and 1926.304 Å are sufficient to establish the strength of the Fe III triplet. The model predicts enough absorption by the Fe III line at 1895.456 Å to explain the observed feature. We can thus only give an upper limit to the Si III column density. This upper limit is less than 10^{17} cm^{-2}. Like Si III λ1895.46, other lines in this spectral region are either weak, or their ion abundance is low. They may affect the details of the model fit when higher S/N spectra are available; they will not affect the general conclusions given here.

This means that, while neither the NAL clouds nor the BAL clouds occult the low-ionization emission region, they must be larger than the projected size of the C^{+2} *zone.* These absorbing clouds must be thin sheets lying perpendicular to the line of sight. The fact that the saturated Fe III narrow lines do not reach zero intensity shows that there is an unocculted continuum source larger than the C^{+2} emission zone.

The Si IV and C IV BAL absorption depth is somewhat uncertain because the CASPEC echelle orders are close together in the UV, and it is difficult to accurately measure the background flux. Yet the data are sufficient to show that any residual intensity at the bottom of the BAL absorption is substantially less than the Si IV and C IV emission to the red of the absorption breaks. Thus the BAL features for these higher ionization lines, unlike that of the lower ionization BAL, occults nearly all the central quasar emission regions; both the emission-line clouds and the continuum sources. The only unocculted emission seen in the C IV BAL absorption occurs at the extreme red edge of the absorption trough. Its velocity extends to only about half the velocity of the Mg II broad emission velocities. Therefore the unocculted portion of the C IV emission line has a low radial velocity compared to Mg II.

The column densities derived for the Si IV and C IV BAL absorptions depend strongly on the input assumptions. Our determinations result from the assumption that it is possible to use the same BAL model for both the low- and high-ionization BAL flows. We can then adjust the column densities of Si IV and C IV until the red wing of the model matches the wavelengths of the rise seen at the red edge of the BAL flows. But high-velocity BAL clouds so weak that they are not seen in the BAL spectra of Mg II and Si II are present and saturated in the blue portions of the Si IV and C IV BAL flows. These clouds substantially extend the width of the high-ionization absorption relative to the low-ionization BAL features. If similar absorption clouds were also present on the red wing of the Si IV and C IV BAL features, they would reduce the column densities we have derived for Si IV and C IV. But the requirement that the lowest column density clouds in our model are saturated in the C IV absorption flow gives an independent lower limit to the C^{+3} column density. If we were to lower the column density of our tabulated model by a factor of ∼10, these high-velocity components of the C IV BAL flow would no longer be saturated and we would expect to see some residual intensity at the positions of the $v = 2740$ km s^{-1} and $v = 3325$ km s^{-1} clouds. The data do not show this; our column density for C IV, which was derived by fitting the red wing of the BAL absorption, is high enough to insure that all nine components of the BAL model are saturated. The high densities we obtained are consistent with our ionization calculations, although these calculations, in themselves, do not provide a sensitive test for the C IV BAL column densities.

We have tried to model the C IV emission line by fitting the red wing of the Mg II emission line to the weak C IV emission line. The strong λλ1560–1585 lines from the a^4F term of Fe II complicate the fitting procedure. But in Figure 6 one can see that (1) the peak wavelength of C IV lies to the blue of 4017 Å, which would be the wavelength of the C IV peak if C IV had the same redshift as Mg II. In addition, (2) the transition to the C IV BAL absorption does not drop at once to zero intensity. There is a narrow "wing" of residual emission next to the BAL absorption edge. This residual emission at the bottom of the C IV BAL feature is much narrower than the Mg II emission line, even if the peak of its emission were at 4017 Å. We conclude that the emission peak of the C IV BEL lies to the blue of the BAL absorption edge and that the BAL flow completely covers the high-velocity portion of the C IV BEL. But there is a weak, low-velocity C IV emission component that is not covered by the C IV BAL feature. If this low-velocity emission line is approximately symmetrical, its peak wavelength cannot lie more than 10 Å to the red of the C IV BAL absorption edge (see Fig. 6).

The C IV NALs are lost in the C IV BAL trough. But if the ratio of the column densities for the NALs and the BALs is the

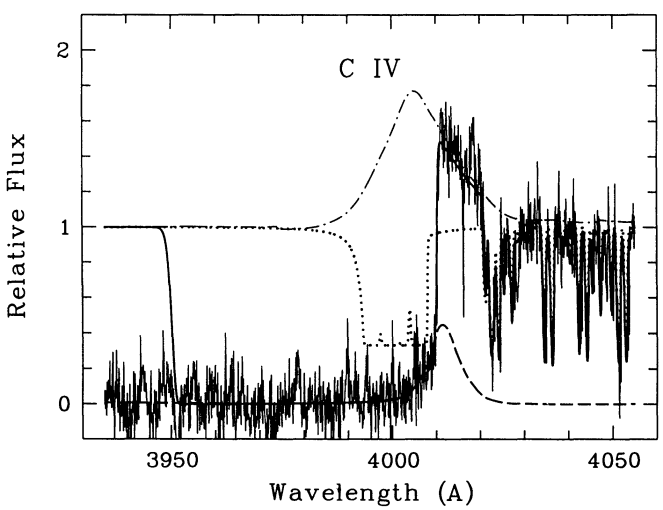

FIG. 6.—C IV BAL region. The dotted line represents possible C IV NAL components if the NAL/BAL ratio is the same as for Fe II. A narrow emission component that is not covered by the BAL absorption may be present and is represented by the dashed line.

same for C IV as it is for Fe II, then the high C IV BAL column density would lead to NAL column densities that would produce C IV NAL damping wings that would extend beyond the C IV BAL absorption edge. Such wings may be present; the unocculted, low-velocity C IV emission line mentioned in the previous paragraph could fill in absorption from rather strong C IV absorption wings that extend to the red beyond the C IV absorption edge.

If the width of the C IV BEL is about the same as that of Mg II, we find that the best fit to the red wing of C IV requires that we shift the peak of the emission-line model ~ 700 km s^{-1} to the blue of the velocity corresponding to the peak of the Mg II and Fe II UV191 emission. The amount of this shift depends on the form and width of the C IV emission line, but it is of the same order as the velocity difference between the Mg II BAL absorption and the Mg II emission peak. Such velocity differences between C IV and Mg II are often found in the emission spectra of quasars (Gaskell 1982; Tytler & Fan 1992). A possible deconvolution of the spectral region near C IV into plausible emission and absorption components is shown in Figure 6. But we emphasize that this suggested deconvolution is uncertain and that much higher S/N spectra of the C IV absorption region are needed in order to increase our confidence in a correct model.

We have far less information about the Si IV region than about the C IV absorption. Our spectra only just cover the Si IV transition region. We have a problem, mentioned above, with the background subtraction, and the S/N of the spectrum at the wavelength of Si IV is poor. The only parameter that can be obtained with high precision is the wavelength of the transition edge. But this is enough to estimate the ionic column density of Si IV.

Because we have good data only for C IV, we have no cross-checks with other ions for absorption clouds with velocities higher than those we can see in the low-ionization BAL features. We have therefore not attempted to model the C IV BAL flow to higher velocities than those seen in the lower ionization BAL flows. When high-resolution, high-S/N spectra that cover the Si IV and N V BAL regions become available, it will be possible to obtain a deeper understanding of the high-ionization BAL flow than is now possible.

Our final conclusions for Si IV and C IV are: (1) The ionization model suggests that high abundance ratios for Si and C relative to Mg are not needed (see § 4.2). (2) The Si IV and C IV BAL clouds are larger than the high-velocity portions of the Si IV and C IV BEL region, but C IV BAL clouds are smaller than a low-velocity emission component. Possibly the C IV emission clouds are moving radially and the BAL clouds do not occult the outer portion of the emission region, or the high-ionization emission clouds are organized into an accretion disk and the BAL clouds do not cover the outer, slowly rotating parts of the disk. The velocity width of the derived unocculted emission clouds is only half the width of the Mg II emission line. Therefore the unocculted C IV emission clouds originate in an emission region that is moving even more slowly than the Mg II emission clouds that are not occulted by the Mg II BAL region. Perhaps also the C IV BAL clouds are more extensive than the Mg II BAL clouds.

Finally, we note here two problems with our model for the absorption lines in the Q0059−2735 spectrum. The first is with the strengths of the low-velocity BAL associated with Si II relative to the strengths of the Si II NALs. This ratio is determined by modeling the absorption lines from the ground term of Fe II. Figure 7 shows the model fit to Si II. The model predicts too little BAL strength unless the NAL column density is increased to the point that the strength of the Si II λ1817.445 fine structure line is too great. The discrepancy is about a factor of 3. One possibility is that the f-value for λ1817.445 that we obtained from Morton (1978) is too high by a factor of ~ 3. A second possibility is that the ratio of BAL absorption to NAL absorption for Si II is higher than for Fe II because Si II is somewhat harder to ionize than Fe II. But the relative strengths of the Fe III NAL and BAL features suggest that there is no great shift from one cloud to another in the relative column densities of the ions that produce the two types of lines.

The second problem, also illustrated in Figure 7, is that the BAL strength is too low for our model to give a good represen-

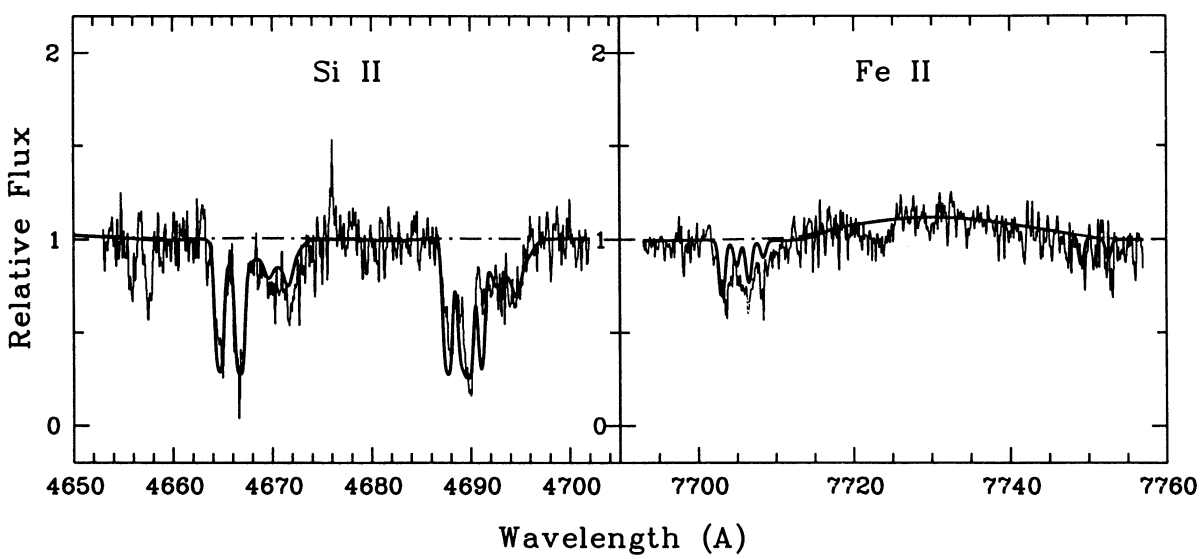

FIG. 7.—Problem transitions Si II and Fe II UV78. For both of these transitions the BAL component is too weak if the NAL component is set to the correct strength. See the text.

tation of the absorption seen in the Fe II UV78 multiplet (excitation potential [EP] = 1.7 eV). Here the discrepancy is about a factor of 4. We have tried to increase the Fe II BAL strength by increasing the column density of the low-velocity clouds and by increasing their excitation temperature. Even with the freedom to choose higher continuum levels, we found that we cannot increase significantly the column density given in Table 3 without compromising the modeling of the ground and low-lying terms. Neither can we increase the excitation temperature without creating difficulties in modeling Fe II UV191 (EP = 2.7 eV) and Fe III (EP = 3.7 eV). With a higher excitation temperature the strength of the Fe II UV191 BAL multiplet becomes too large and the column density of Fe^{+2} becomes so low that it is no longer possible to obtain sufficient column density, even with an infinite excitation temperature, for the higher velocity Fe III BAL clouds. The oscillator strengths for Fe II UV78 were taken from Fuhr et al. (1988). An increase in the *f*-values of the $\lambda\lambda$2985.6, 2986.4 lines by a factor of 4 would solve the problem.

Si II λ1817.445 and Fe II UV78 models present the only serious problems that we have encountered in understanding the absorption spectrum of Q0059−2735.

4. IONIZATION MODELS

4.1. *The Physical Conditions of the NAL Clouds*

4.1.1. *Ionization Structure of the NAL Material*

In order to estimate the physical conditions in the clouds producing the NALs we considered the following simple model: a homogeneous slab of a column density N at the distance r from the source with the UV luminosity $L_\nu = \nu^{-1} L$. The column density of the H II Strömgren layer is

$$N_S = L(4\pi r^2 I_H \alpha n)^{-1} = 10^{23} U \text{ cm}^{-2} , \quad (1)$$

where I_H is the hydrogen ionization potential and U is the ionization parameter, i.e., the ratio of the density of photons with energies above 1 ryd to the hydrogen density (n). At the illuminated side of the H II layer lies an He III layer with a column density $N_{\text{He III}} \approx 6 \times 10^{21} U$ cm^{-2} and an He II layer with $N_{\text{He II}} \approx 5 \times 10^{22} U$ cm^{-2}.

The ionization of hydrogen in the H I region behind the Strömgren layer is actually rather high. It is determined by two main processes: photoionization from the second level and collisional nonthermal ionization from the ground level by photo- and Auger electrons (cf. Collin-Souffrin & Dumont 1986). By taking into account only nonthermal ionization and neglecting any additional photoionization from the second level, we will obtain a lower limit of the ionization degree of hydrogen (x) in the H I zone. This can be done in the approximation of the complete absorption of the X-ray and UV flux at the optical depth $\tau = 1$. We will use a standard cross section for the photoabsorption, $\sigma = 2 \times 10^{-22} E_{\text{keV}}^{-8/3}$ in the region $h\nu \geq 100$ eV, and assume that one ionization of hydrogen atom requires $3I_H(1 - x)^{-1}$ of the deposited energy, where the factor containing x approximately takes into account the increasing role of Coulomb heating in the ionization losses when the degree of ionization is high, $x > 0.1$. Equating the corresponding ionization and recombination rates one can find the ionization degree of hydrogen in the H I region ($N > N_S$):

$$x_H = C(N/N_S)^{-1/2} , \quad (2)$$

where the factor $C = 0.3$ for $N \approx N_S$ and $C = 0.4$ for $N \gg N_S$. This estimate shows that for a wide set of parameters the ionization degree exceeds 0.3 in the H I region close to the H II–H I interface. This conclusion is in general agreement with detailed photoionization models (cf. Collin-Souffrin & Dumont 1986).

4.1.2. *Ionization of Metals*

In the He III zone Mg, Si, and Fe are strongly ionized, and the contribution of this zone to the column density of low-ionized species of these metals is negligible. In the He II zone the most abundant ion of Mg is Mg III (EP = 80 eV), while Si and Fe, with ionization potentials of the doubly ionized ion equal to 35 and 30 eV, respectively, will be in the triply ionized states. On the other hand, in that part of the H II zone where He is neutral, Mg, Si, and Fe will be only doubly ionized. If the column density of the slab exceeds that of the Strömgren layer, the H I region may become the major contributor to the column density of Si II and Fe II.

In Table 4 we list the column density for both the Strömgren layer and for the H I region of those ions with distinctive NALs, including an upper limit for the unobserved Mg I. Solar abundances were assumed. Mg I is included because it imposes an important upper limit on the relative width $\xi = N_{\text{H I}}/N_S$ of the H I region. Available data on photoionization cross sections (Reilman & Manson 1979) and recombination rates (Shull & Van Steenberg 1982) have been used for the calculation of the ionization degree. Both, radiative and dielectronic recombination rates were used, and the electron temperature was taken to be 10^4 K. Comparing column densities of Si II and Fe II in Table 4 with observational data in Table 3 one readily sees that it is not possible to obtain the column density of the two strongest components, $N_{\text{Si II, Fe II}} \approx 10^{16}$ cm^{-2}, in the Strömgren layer. This indicates that the major contributions to the column densities of Fe II and Si II belong to the H I zone. The extension of the H I region required to reproduce the observed column densities is very small. The upper limit of the column density of Mg I, $N_{\text{Mg I}} < 10^{13}$ cm^{-2}, taken together with the lower limit of the ionization degree, $x > 0.3$, places a severe constraint on the relative width of the H I zone: $\xi < 0.03$. With this limit on ξ and the observed column densities of Si II and Fe II (10^{16} cm^{-2}), we immediately obtain from Table 4 (col. [2]) a lower limit to the ionization parameter $U > 0.1$, or

$$n < 1.2 \times 10^8 L_{46} r_{19}^{-2} \text{ cm}^{-3} , \quad (3)$$

where L and r are expressed in 10^{46} ergs s^{-1} and 10^{19} cm, respectively.

An upper limit on the ionization parameter can be determined using only the fact that low-ionization gas exists. As shown by Begelman, de Kool, & Sikora (1991), the thermal balance sets an upper limit to the ionization parameter, $U < 4$. This corresponds to the inequality

$$n > 3 \times 10^6 L_{46} r_{19}^{-2} \text{ cm}^{-3} . \quad (4)$$

The upper limit $U < 4$, taken together with the observed

TABLE 4

COLUMN DENSITIES PREDICTED FROM PHOTOIONIZATION MODEL OF NAL GAS

Zone (1)	Mg^0 (2)	Fe^+ (3)	Fe^{++} (4)	Si^+ (5)
H I zone	$10^{15} x\xi$	$3 \times 10^{18} U\xi$		$3 \times 10^{18} U\xi$
H II zone.....	$2 \times 10^9 U^{-1}$	6×10^{14}	$1.5 \times 10^{18} U$	10^{14}

column density 10^{16} of Fe II and Si II, imposes a lower limit on the relative width of the H I layer, $\xi > 10^{-3}$ (see Table 4).

The observed column density of Fe III (cf. Table 3) in the excited $a\,^7P$ term (EP = 3.7 eV) (2–4) $\times$ 10^{14} cm^{-2} requires the total column density $N_{\rm Fe\,III} \approx 10^{17}$ cm^{-2}, provided the excitation temperature is $\approx$7000 K. This column density for the Fe III NAL clouds can be reached in the Strömgren layer if $U \approx 0.1$ (see Table 4). The latter is marginally consistent with the lower limit $U > 0.1$ obtained above. The weaker, low-velocity NAL components of Fe II and Si II (0 km s^{-1} and 130 km s^{-1}) cannot be produced in the Strömgren layer. Additional H I material is required for these lines to be seen.

4.1.3. *The Excitation Mechanism*

The population of the metastable Fe II NAL terms corresponds to an excitation temperature of $\sim 10^4$ K. The excitation mechanism may be collisional excitation of Fe II since the electron temperature in the H I zone is also $\sim 10^4$ K. Recalling that the radiative transition probability of $a\,^4D$ is 0.006 s^{-1}, collisional excitation requires the electron density to be $n_e > 10^6$ cm^{-3}.

Radiative transitions may also contribute to the excitation of Fe II. The metastable levels of Fe II can be excited radiatively either by a photoionization with subsequent recombination, or by bound-bound transitions via other upper levels. In order for the recombination rate to compete with the de-excitation rate of the metastable level $a\,^4P$ ($A = 0.002$ s^{-1}), the electron density must exceed 10^{10} cm^{-3}, which, as we will see later on, is unreasonably high.

The chain of bound-bound radiative transitions from the ground level $a\,^6D$ to $a\,^4P$ via the third upper level (symbolically, 1–3–2) occurs only via intercombination transition, e.g., $a\,^6D$–$z\,^6D^0$–$a\,^4P$, which have the oscillator strength $f \approx 10^{-4}$. In order to maintain high excitation temperature the radiative rate 1–3–2 must be competitive with the rate of spontaneous decay A_{21}. This suggests that the rate of the radiative transition 2–3 with the energy E_{23},

$$R_{23} = \frac{L_\nu \sigma f_{23}}{4\pi r^2 E_{23}} = 5.33 f_{23} L_{46} r_{20}^{-2} \left(\frac{E_{23}}{1\ \text{eV}}\right)^{-2} \text{s}^{-1}, \qquad (5)$$

must be large compared to $A_{21} \approx 0.002$ s^{-1}. With $f_{23} \approx 10^{-4}$ and $E \approx 3$ eV we obtain the corresponding upper limit on the distance to the NAL material $r < 2 \times 10^{19}$ cm. If should be emphasized that due to the specific level structure of Fe II the rates of the direct and inverse Rosseland cycles are comparable and as a result the excitation temperature of the metastable levels can be close to the color temperature of the continuum (Chugaĭ 1980).

The alternative process of the excitation of the $a\,^4P$ term may involve both collisional excitation of $a\,^4F$ (0.3 eV) and subsequent radiative permitted transitions of the type 1–3–2 (where "1" refers to the term $a\,^4F$, while the ground term $a\,^6D$ is designated here as "0"). For electron temperature $\approx 10^4$ K the population of term $a\,^4F$ is comparable to that of the ground term. Therefore the collisional-radiative mechanism can also provide the high excitation temperature of the term $a\,^4P$. In this case the radiative rate of transition 2–3 (UV36, $f_{23} \approx 0.04$) must be high, $pR_{23} > A_{20}$ (where $p \approx 0.02$ is the branching ratio for the transition 3–2). According to equation (5) this requirement leads to the upper limit of the distance $r < 5 \times 10^{19}$ cm. Yet, the collisional de-excitation rate for the term $a\,^4F$ must exceed the net radiative rate 1–3, which in its turn is greater than A_{20}. With a typical collisional coefficient for Fe II, $q \approx 3 \times 10^{-9}$ cm^3 s^{-1}, and with $A = 0.002$ s^{-1} we obtain the lower limit of the density $n_e > 10^6$ cm^{-3}. This mechanism has no advantage over purely collisional excitation.

In principle one might distinguish between purely collisional and radiative excitation by noting that excitation by a blue continuum will result in a high excitation temperature compared to collisional excitation in an H II region gas. For example, if $T_{\rm exc} > 20{,}000$ K for the metastable levels of Fe II, radiative pumping rather than collisional excitation is indicated. The excitation temperatures listed in Table 2 suggest that radiative excitation may dominate over collisional excitation in the high-velocity BAL flow, while collisional excitation may dominate in the case of the low-velocity BAL flow and in the NAL clouds. Therefore, both of these excitation mechanisms for Fe II may play a role in the Q0059−2735 absorbing clouds.

4.1.4. He II λ1640 *Absorption*

In spite of a high excitation potential, the second level of He II can be sufficiently populated by radiative processes to produce observable absorption lines. We have not detected He II λ1640 absorption, which implies an upper limit of the column density in the second level of $N_2 < 3 \times 10^{12}$ cm^{-2}. This upper limit may impose an important constraint on the parameters of the NAL material.

Let us consider a slab illuminated by the continuum flux F_ν with the optical thickness τ_0 in the resonance He II λ304 line. We assume that the population of the second level is controlled by the radiation in the resonance transition. In fact the collisional excitation for all reasonable densities and electron temperatures is negligible compared to the excitation by the direct continuum radiation. As for the collisional de-excitation, the critical electron density may be estimated in the following way. For the column density of He II (see § 4.1.1) $N_1 = 5 \times 10^{21} U$ and $b = 17$ km s^{-1}, the optical depth in the λ304 line is $\tau_{12} = 1.5 \times 10^8 U$. This means that the scattering in Lorentz wings dominates, and the photon escape probability may be written as $\beta_{12} \approx 1/\tau_{12}$. The critical electron density with the collisional strength $\Omega_{12} = 0.25$ is then $n_{e,\rm cr} = A_{21}\beta_{12}/q_{21} \approx 10^{10} U^{-1}$ cm^{-3}. The following analysis of the radiative excitation of He II suggests that the electron concentration is below this value.

In order to determine the column density of He II in the second level we will use an important symmetry property of the source function in the resonance transition. If the intensity of the incident radiation is independent of the direction, then

$$S(\tau) + S(\tau_0 - \tau) = I \qquad (6)$$

(here we omit frequency dependence). This relation was derived from the transfer equation for the case of complete redistribution function (Ivanov 1973). However, it can be also generalized on the case of the arbitrary redistribution function. To demonstrate that, we use a simple but in some cases very efficient method (cf. Chugaĭ 1992).

Let us imagine that the resonance scattering slab is placed in the two-sided isotropic radiation field with the intensity I. It is obvious that the steady state intensity inside the slab will be I in any point. On the other hand, this local radiation can be represented by the superposition of the incident and diffuse radiation field produced by the radiation falling on either side of the slab; i.e., $I = I(\tau) + I(\tau_0 - \tau)$. Bearing in mind that for the purely radiative case $S(\tau) = I(\tau)$ we thus immediately obtain equation (6). This result does not suggest any particular

form of the redistribution function. Of course, we neglect the redistribution caused by the recoil effect, which does not affect noticeably the excitation degree of the second level.

Integrating equation (6) over τ gives the column density of the excited He II in the second level:

$$N_2 = N_1 \frac{c^2}{4h\nu^3} \frac{g_2}{g_1} I \,. \tag{7}$$

Approximating the intensity I by $F_\nu(4\pi)^{-1}$ and substituting $N_1 = 5 \times 10^{21}$ cm^{-2}, we obtain from the absence of He II $\lambda 1640$ (i.e., $N_2 < 3 \times 10^{12}$ cm^{-2}) the lower limit for the distance of the NAL material:

$$r > 3.6 \times 10^{18} \left(\frac{n}{10^7 \text{ cm}} \right)^{-1/4} \text{cm} \,, \tag{8}$$

which is not sensitive to the density parameter.

4.1.5. *The Absence of Acceleration*

The NALs in Q0059−2735 have not shown any evidence for acceleration during the period of our observations. The upper limit on the acceleration is 0.03 cm s^{-2}. As we saw, the column density of NAL structures is close to the column density of the Strömgren layer. This fact leads us to a simple expression for the acceleration due to the photoabsorption of continua:

$$a_{\text{rad}} = \frac{\alpha n_e \text{Ry}}{c m_{\text{H}}} = 1.1 \times 10^{-10} n_e \text{ cm s}^{-2} \,. \tag{9}$$

From the observational limit $a_{\text{rad}} < 0.03$ cm s^{-2} one obtains $n_e < 3 \times 10^8$ cm^{-3}. The derived upper limit presumes that radiative acceleration dominates gravitational acceleration. This is the case when

$$n_7 r_{19}^2 > 1.4 M_9 \,, \tag{10}$$

where M_9 is the central mass of the QSO in $10^9\ M_\odot$.

The above considerations suggest that NAL structures are frozen into the flow. The absence of the noticeable drift of NALs may also invoke an alternative picture, in which NAL structures linked with a fixed geometrical position of the Strömgren layer in the steady accelerating flow. The flow may be supplied by the local source of matter, e.g., dense clouds, accretion disk, stars (e.g., the model by Voit et al. 1993). However, in this case it is not easy to understand the fact that the steady flow beyond the Strömgren layer (i.e., in the H I region) does not contribute to NAL absorption. Proponents of such models should suggest some mechanism for a sudden "disappearance" of the H I absorbing material behind the edge of the Strömgren layer.

4.2. *Photoionization Modeling of the BAL Flow*

It has been shown in § 3.2 that the BAL flow has the same velocity structure in different lines. The flow can then be understood as the superposition of different regions at definite velocities relative to the QSO. The column densities for these regions are given in Tables 2 and 3. It can be seen that the column density ratios in the three lowest velocity components are very similar. Therefore, we use the column densities derived for the cloud 5 (see Table 2) to constrain photoionization models. The latter cloud accounts for about one-third of the total column density of the BAL flow in any observed absorption. The physical conditions derived for this cloud should be representative of the physical conditions prevailing in the flow.

4.2.1. *Constraints from the N(Al II)/N(Al III) Ratio*

We use for aluminum the set of atomic data given by Petitjean, Rauch, & Carswell (1994). The latter authors have shown that it is difficult to obtain the large N(Al III)/N(Al II) column density ratios as observed in Q0059−2735 (see their Fig. 7). This is mainly due to the rapid dielectronic recombination rate of Al II at high temperature. The latter has been extrapolated from Si III and Mg I (Aldrovandi & Péquignot 1973) and is given by the expression $\alpha_{\text{diHT}} = 0.05 T^{-1.5} \exp(-87{,}000/T)$ cm^3 s^{-1}. The total Al II recombination coefficient increases quickly with temperature and is $\alpha_{\text{tot}} = 3.9 \times 10^{-12}$, 1.26×10^{-11}, and 2.33×10^{-10} cm^3 s^{-1} at $T = 5000$, 10,000, and 20,000 K, respectively.

The density ratio N(Al III)/N(Al II) is proportional to the ionization parameter U and, for a given value of U, increases with decreasing temperature. For a power-law ionizing spectrum of index -1 and $U = 0.05$, we obtain N(Al III)/N(Al II) $\sim A(T/5 \times 10^3)^\beta$ with $A = 72.2$, $\beta = -1.7$ for $5 \times 10^3 < T < 10^4$ K and $A(T/10^4)^\beta$ with $A = 22.2$, $\beta = -4.2$ for $10^4 < T < 2 \times 10^4$ K.

Large values of the ionization parameter can explain large column density ratios N(Al III)/N(Al II). However, as the ionization potential of Al III is 28.44 eV, large ionization factors also imply low N(Al III)/N(Al) ratios. Therefore, for Al abundance not too much in excess of the solar abundance, N(Al III) column densities as large as those observed suggest a steep ionizing spectrum and low temperatures ($T \sim 10^4$ K) in the Al III region.

4.2.2. *The Iron Problem*

Because the broad Fe II absorptions are weak and blended, the column densities quoted in Table 3 are somewhat uncertain. However, Fe II must be present with column densities of the order of 5×10^{14} cm^{-2}. The arguments in favor of the presence of Fe II in the BAL flow are the consistency of the broad features needed to reproduce the four different Fe II absorptions and the agreement of the Fe II model with the BAL model for the other ions.

The other singly ionized ions, such as Mg II, Si II, and Al II, that are present are easily produced even when hydrogen is ionized. Si II, Si III, and Al II have recombination coefficients larger by an order of magnitude than the similar coefficients for Fe II and Fe III (Aldrovandi & Péquignot 1978; Shull & Van Steenberg 1982). Beyond the He II boundary, and for a continuous power-law ionizing spectrum in the interval 13.6–54.4 eV, Mg III and Fe IV are the dominant magnesium and iron species. Thus, to a first approximation we can write

$$\frac{\text{Fe}}{\text{Fe III}} \frac{\text{Mg II}}{\text{Mg}} \sim \left(\frac{30.6}{15} \right)^{-\eta} \frac{\sigma_{\text{Fe III}}}{\sigma_{\text{Mg II}}} \frac{\alpha_{\text{Mg II}}}{\alpha_{\text{Fe III}}} \,, \tag{11}$$

where η is the opposite of the power-law ionizing spectrum index, $F = F_0(\nu/\nu_0)^{-\eta}$, α the total recombination rate and σ the ionizing cross section at the ionization limit (30.6 eV for Fe III and 15 eV for Mg II). For $\eta = 1$ the ratio is ~ 4. As iron and magnesium have approximately the same solar abundances, Fe III and Mg II should have about the same column densities if the abundance ratio is solar. This holds up to the hydrogen boundary. Beyond that boundary, and because of the very similar ionization potentials (13.6 and 15 eV, respectively), hydrogen and magnesium recombine to H I and Mg II; in this region, because of charge exchange reactions with H I, the

dominant ions of Fe and Si are Fe II and Si II. This happens as soon as H I/H ≥ 0.05. Since the N(Al III)/(Al II) and N(Si III)/N(Si II) ratios are both of the order of 10, the optical depth of the BAL clouds in Q0059−2735 cannot be much in excess of 10. Therefore, H I never completely recombines (see also Voit et al. 1993). There is thus a thin layer in the cloud where iron is Fe II but where hydrogen has not completely recombined.

There are thus two possibilities: the total H I optical depth of the cloud might be of the order of 10; then Fe II would be produced in a very thin layer. In this case the column density would be very sensitive to the H I column density and we would expect larger variations than we see in the N(Fe II)/N(Fe III) ratio from one component to the other. Alternatively, the H I optical depth is smaller, and hydrogen is everywhere highly ionized; then iron must be overabundant with respect to magnesium (see § 4.2.4).

4.2.3. *Abundance Estimates*

The large N(Al III)/N(Al II) ratio shows that hydrogen is certainly ionized throughout the entire cloud. From this, and because H I and Mg II have similar ionization potentials, we can estimate the magnesium abundance. Between the He II and H I boundaries, Mg III and H II should dominate so that

$$Z(\mathrm{Mg}) \sim 2 \frac{\alpha_{\mathrm{H\,I}}}{\alpha_{\mathrm{Mg\,II}}} \frac{\sigma_{\mathrm{Mg\,II}}}{\sigma_{\mathrm{H\,I}}} \frac{N(\mathrm{Mg\ II})}{N(\mathrm{H\ I})}, \qquad (12)$$

where the notation is the same in equation (11) and Z(Mg) is the abundance by number for magnesium relative to hydrogen. With N(Mg II) $= 2 \times 10^{15}$ cm^{-2} and N(H I) $= 10^{18}$ cm^{-2} we find that the magnesium abundance should be about solar. This conclusion was reached earlier by Voit et al. (1993).

It has been suggested that the abundances in BAL systems may be in excess of solar by very large factors (Turnshek 1988), though Kwan (1990) suggests that the overabundances may be no more than two. However, in the very center of QSOs where the BALs and BELs presumably arise, the abundances could be in excess of solar by a large factor. Hamann & Ferland (1992) have estimated from the observed N V/C IV emission-line intensity ratio that nitrogen should be enhanced relative to carbon by a factor of 2–10 in the BEL region of high-redshift quasars and that high abundances (3–14 times solar) are required to explain this. From detailed computing of galaxy evolution and chemical enrichment, Matteucci & Padovani (1993) have shown that in elliptical galaxies and bulges of spirals solar abundances are reached in a few 10^9 yr and that N, Si, and Fe are expected to be overabundant as compared to the other elements. The excess of iron suggested in § 4.3.2 could help resolving the so-called Fe II problem of BEL regions (see, e.g., Netzer & Wills 1983; Wills, Netzer, & Wills 1985; Collin-Souffrin & Lasota 1988).

4.2.4. *Detailed Modeling*

We have used the detailed photoionization code NEBULA (Péquignot, Aldrovandi, & Stasińska 1978; Petitjean, Boisson, & Péquignot 1990), which computes the ionization structure of a spherical nebula surrounding a central source of ionizing radiation. The diffuse ionizing flux produced by recombination in the nebula itself is computed exactly along 20 outward directions. A detailed treatment of the flux from the diffuse emission is necessary since diffuse flux is as important as the flux from the central source when the optical depth is close to one. The most important parameters for the ionization modeling are the absolute value of the ionizing flux at the Lyman limit, the shape of the ionizing spectrum, and the element abundances. The ionization structure of the slab is defined by the ionization parameter $U = Q/n_{\mathrm{H}}c$, where Q is the flux of photons with energy larger than 13.6 eV, n_{H} the hydrogen density, and c the speed of light. The hydrogen density has been varied between 10^6 and 10^8 cm^{-3} without any significant change in the models. The solar values for abundances are taken to be 1, 0.083, 4(−4), 1(−4), 6.9(−4), 7.4(−5), 3.5(−5), 3.5(−5), 2.5(−6), and 3.2(−5) for H, He, C, N, O, Ne, Mg, Si, Al, and Fe, respectively (de Boer, Jura, & Shull 1987).

The observed and computed column densities are given in Table 5. In the following we use the notation [X/Y] = log [Z(X)/Z(Y)] − log [$Z_\odot$(X)/$Z_\odot$(Y)], where X and Y are any elements and Z is the abundance of those elements by number relative to hydrogen.

We first investigate models with constant density and a double power law ionizing spectrum with no intensity discon-

TABLE 5

OBSERVED AND MODELED COLUMN DENSITIES FOR BAL GAS (in cm^{-2})

Element	Observed	M1	M2	M3	M4
$\alpha(<54.4$ eV)[a]	...	0.8	3.0	3.0	3.0
$\alpha(>54.4$ eV)	...	3.0	3.0	3.0	3.0
U[b]	...	0.1	0.2	0.2	0.2
[C/H]	...	0.3	0.3	0.3	0.3
[Fe/C]	...	1.0	1.0	1.0	0.0
ΔT[c] (10^4 K)	...	1.80–1.40	1.65–1.20	1.65–1.05	1.70–1.10
H I	...	2.0×10^{18}	6.9×10^{17}	2.7×10^{18}	2.0×10^{18}
C IV	2.4×10^{18}	2.4×10^{18}	7.6×10^{17}	7.6×10^{17}	8.0×10^{17}
Mg II	2.2×10^{15}	2.5×10^{15}	1.9×10^{15}	6.9×10^{15}	4.4×10^{15}
Al II	2.2×10^{14}	5.2×10^{14}	5.6×10^{14}	2.2×10^{15}	1.4×10^{15}
Al III	4.8×10^{15}	8.4×10^{14}	4.8×10^{15}	7.9×10^{15}	5.1×10^{15}
Si II	2.0×10^{15}	8.0×10^{14}	2.9×10^{15}	1.3×10^{16}	6.6×10^{15}
Si III	$<10^{17}$	2.1×10^{16}	2.2×10^{17}	2.8×10^{17}	2.2×10^{17}
Si IV	4.4×10^{17}	4.8×10^{17}	2.5×10^{17}	2.5×10^{17}	2.7×10^{17}
Fe II	5.0×10^{14}	5.6×10^{12}	5.4×10^{13}	2.3×10^{16}	3.7×10^{14}
Fe III	4.0×10^{16}	5.8×10^{15}	4.5×10^{16}	4.9×10^{17}	1.0×10^{16}

[a] Ionizing spectrum index.
[b] Ionization parameter.
[c] Temperature range through the cloud.

tinuity. The energy index is given the values $\eta = -0.8$ and -3 below and above the He II ionization potential, respectively. This is close to the shape of the standard active galactic nucleus spectrum (Mathews & Ferland 1987). Except for Fe, which is considered to be a factor of 10 overabundant, the abundance ratios are taken to be solar. The solutions that we can obtain are typically those of model M1 in Table 5. It can be seen that the C IV and Mg II column densities are well fitted. However, N(Fe II) is too small by two orders of magnitude, and the ratio N(Al III)/N(Al II) is 15 times too small. The latter ratio is a consequence of the high temperature throughout the cloud ($T > 13{,}000$ K).

Considering density variations through the cloud cannot improve the fit since, with the same kind of ionizing spectrum, Al II is produced in the same region as Fe II, and N(Al II) would become too large. Apart from increasing the iron abundance, we can decrease the relative number of Fe III ionizing photons ($h\nu > 30.6$ eV). A break in the ionizing spectrum at energy in the range 20–30 eV is difficult to explain by absorption through a cloud of the kind we observe. Column densities of the order of 10^{17} cm^{-2} for He I or 10^{18} cm^{-2} for C II, N II, or O II are needed to produce a break of a factor larger than 10 at 24.6, 24.3, 29.6, or 35.1 eV, respectively. A second possibility is that an additional source of ionizing flux, possibly from mixing layers, increases the relative number of photons with energy smaller than 30.6 eV. Still another alternative is that the slope of the ionizing flux from the QSO could be much larger than the value 0.8 that we used in the first model. In model M2 we try a steeper slope for the ionizing continuum. It can be seen in Table 5 that the N(Al III)/N(Al II) ratio is close to the observed ratio. But N(C IV) is too small by a factor of 2 and the Fe II column density is too small by a factor of 10. But a small increase in the H I column density induces a large increase in N(Fe II) (see § 4.2.2). This is illustrated by model M3, which is identical to model M2 except that the N(H I) column density is 3 times larger than for M2. While the column densities of the singly ionized ions are generally too large by a factor of 2, the striking difference is that N(Fe II) is now 20 times in excess of observation. Also note that the N(Al III)/N(Al II) ratio is now very much too small.

This suggested that we could fine-tune a model with solar iron abundances. The results of our attempt are shown as model M4. This model is satisfactory except that the N(Al III)/N(Al II) ratio is still too small. The best model must lie between models M2 and M4.

We thus conclude that, within the uncertainties inherent to the column density determination, the set of column densities observed in the broad absorptions of Q0059−2735 can be reproduced in the framework of photoionization. We derive carbon abundances of the order of the solar value and probably iron abundance in excess of the carbon abundance by a factor smaller than 10. The ionizing spectrum must be steep to minimize the relative number of photons with energy larger than the Fe III ionization potential. We use in our best model a power law of index -3. The ionization parameters needed in the models are of the order of 0.2; about the same as estimated for the NAL clouds discussed in § 4.1.2.

5. DISCUSSION

Our analysis of the NAL spectrum leads us to some useful constraints for the parameters of NAL material. For an adopted QSO luminosity of $\nu L_\nu = 10^{46}$, these can be shown in a "density–distance" plane (Fig. 8). The boundaries correspond to inequalities (3), (4), and (8) and the limits on the density. The lower density limit is set by the need for collisional excitation of Fe II at large distances, $r \geq 2 \times 10^{19}$ cm, where the radiative excitation fails. The upper density limit is imposed by the absence of acceleration. In fact, for the allowed range of n and r at the upper border, the radiation pressure dominates gravitational attraction if the central mass $M < 10^9\ M_\odot$.

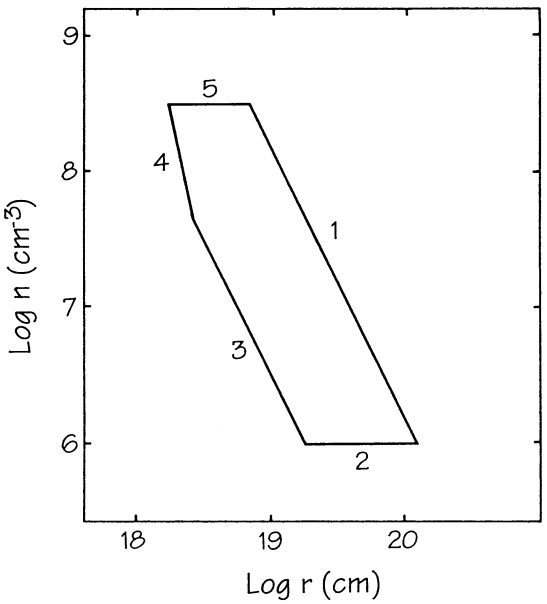

FIG. 8.—Parameters of the narrow absorption material in a density–radius plane. The allowed values for solar abundances are restricted by (1) absence of Mg I line, (2) requirement of the collisional or collisional-radiative population of Fe II levels, (3) existence of cool material, (4) absence of He II λ1640 line, and (5) absence of noticeable acceleration.

A striking common property of the NAL and low-ionization BAL clouds in Q0059−2735 is that their column densities coincide with the column density of the Strömgren layer (eq. [1]). However, the most amazing fact is that this equality holds to an accuracy of $O(10^{-2})$! The fact that low-ionization BAL and NAL clouds should be somewhat larger than Strömgren column density can be easily explained by the observational selection: smaller column densities do not produce low-ionization absorption lines. But observational selection is an unsatisfactory explanation for the fact that we do not see any clouds in Q0059−2735 with column densities significantly, say 10%, larger than the Strömgren column density. Any explanation of this observation should invoke some fine-tuning mechanism for the "cutoff" H I layer unless it is thinner than some limit, say 1%–2% of the Strömgren column density. Obviously, such a mechanism must somehow involve the Lyman continuum cutoff. One possibility is that at the H II/H I boundary the Lyman continuum cutoff creates pressure and density gradients that lead to the development of convective instabilities. This instability should destroy any H I layer with a width exceeding a critical value $O(10^{-2}\ N_S)$. Of course, only a detailed study of this problem may clarify the nature of the column density cutoff. Yet, the suggested mechanism might also naturally explain (1) why NALs of Fe II are such a rare phenomenon among QSOs with low-ionization BALs and (2) why the Fe II lines show significant residual intensity. The answer to the first question suggests that the column density of the H I layer required for Fe II to be observed is generally

beyond the stability limit of this layer. So, such a thick H I layer generally does not survive. In those rare cases when we see a relatively thick H I layer it will be basically destroyed and therefore be clumpy. The clumps will produce Fe II absorptions with a finite residual intensity, since clumps have relatively low covering factor.

The residual emission in the NALs may be explained in two different ways: (1) The residual intensity might be produced by the partially occulted central continuum source with the radius $R_c \sim 10^{15}$ cm. In this case we have suggested that the unocculted source could be a thermal source with a temperature in the range 13,000–17,000 K. (2) Alternatively, the central continuum source could be completely occulted, while the residual intensity is in fact a quasi continuum composed by Fe II UV emission lines emitted by the BEL region. In normal QSOs Fe II contributes perhaps 20% of the continuum in the range 2000–3000 (Wills et al. 1985). However, those BAL quasars with Mg II and Al III absorption show unusually strong Fe II emission (Weymann et al. 1991). If a strong Fe II quasi continuum were present in Q0059−2735, it might be possible for the residual intensity in the NAL line bottoms to reach 30%–40% and not 20%. However, we believe that any contribution to the residual intensity of the narrow lines must be minor, because saturated narrow lines, such as Si II and Ni II, which lie in spectral regions where there are no strong Fe II transitions, have residual intensities similar to those seen in the narrow Fe II lines, which lie in regions where there are strong Fe II multiplets. In either version of the origin of the residual intensity, the transverse size of the NAL cloud should approximate the radius of the central continuum in order to occult the continuum source almost completely, $a_t \approx R_c \sim 10^{15}$ cm. The high electron density, together with the relatively low ionic column density, shows that the NAL clouds are thin sheets.

The similarity between the radial velocities of the Fe II and Fe III NAL and BAL systems suggests a close physical relationship between the two-cloud systems. This, together with the fact that clouds producing low-ionization absorption, both NAL and BAL, have low velocities and high column densities, while the high-velocity absorbers have lower column density and higher ionization, favors flow models in which material is ablated from low-velocity, cool, dense clouds. This model recently has been proposed for the interpretation of low-ionization and high-ionization BAL systems in QSOs (Voit et al. 1993). It is also generally consistent with the pattern that the NAL clouds have high residual intensity in the line bottoms, since small NAL clouds would only partially occult the continuum source. In contrast, the BAL flow must have a much larger transverse size than the narrow-line region in order to occult all the continuum source, but they must not be so large as to occult the outer, low-ionization BEL region. As the ionization of the BAL flow increases, the cloud cross section increases, and finally, nearly the entire central region of Q0059−2735 is occulted.

The rate of mass supply required to produce a strong NAL component existing during at least the dynamic time r/v is

$$\dot{M} = (0.3\ M_\odot\ \mathrm{yr}^{-1})\left(\frac{\Omega}{4\pi}\right) r_{19}\, v_7\, N_{22}\ , \qquad (13)$$

where Ω is the solid angle subtended by the NAL flow, r_{19} is the distance to the QSO nuclei, v_7 is the velocity of the NAL cloud in 10^7 cm s^{-1}, and N_{22} is the column density in 10^{22} cm^{-2}. For $\Omega/4\pi \approx 0.1$ and $r_{19} \approx v_7 \approx N_{22} \approx 1$, one gets $\dot{M} \approx 0.1\ M_\odot$, which is rather moderate compared with a standard estimate of the accretion rate $\approx 2\ M_\odot$ yr^{-1}. The estimated mass would be even lower if $\Omega/4 < 0.1$.

The origin of the dense material which supplies BAL and NAL flows is unclear. The lifetime of the low-velocity NAL material may hardly significantly exceed 10^2 yr, the time required to accelerate material up to velocity 100 km s^{-1} for a density of $\sim 10^7$ cm^{-3} (see eq. [9]). This suggests that low-ionization NAL clouds have recently been exposed to the intense UV radiation of the quasar. The latter could happen, e.g., if Q0059−2735 has just turned on, or if low-ionization clouds have recently moved into the radiation field of Q0059−2735. In that case we are lucky to observe the initial phase of the removal of circumnuclear material in this particular QSO, and this may explain the rarity of QSOs similar to Q0059−2735.

Another possible mechanism for suddenly placing relatively low ionization gas into the quasar radiation field would be for an SN explosion in the outer quasar accretion disk to blow low-ionization gas out of the plane of the disk. (See Artymowicz, Lin, & Wampler 1993 for a discussion of star trapping and SN explosions in quasar accretion disks.) In this case, the metallicity of the absorption lines in Q0059−2735 should be a fair sample of the metallicity of the core region of a quasar. If NAL absorbers are identified with the disk material swept up by SN explositions the supernova remnant (SNR) material must be decelerated to the velocities of the order of 10^2 km s^{-1} in a short time comparable with the lifetime of NAL structures, $t \leq 100$ yr. For a SNR expanding at the snowplow stage (Shull 1980) the deceleration to 100 km s^{-1} on a timescale of 100 yr requires an ambient density of $\approx 10^7$ cm^{-3}, in which case the radius of the SNR after 100 yr is $\approx 10^{17}$ cm. The probability for a line of sight lying close to the equatorial plane to intersect such a SNR at $r \approx 10^{19}$ cm is roughly $0.5(l/r) \approx 0.005$. Four velocity components could be seen if the line of sight intersects two SNRs. This suggests that the number of SNRs in the equatorial plane is of the order of $N = 2\pi(r/l) \approx 600$. The required rate of SN explosion is 6 yr^{-1}. This should be compared to the maximum allowed rate of SN explosions in QSOs. On the timescale 10^8 yr, only SN II's would contribute. Producing one SN II requires the conversion during massive star evolution of roughly 3 $M_\odot$ of hydrogen into He with the release of $E \approx 3.6 \times 10^{52}$ ergs per SN II. The total optical and IR luminosity of a QSO, $L \approx 10^{46}$ ergs s^{-1}, sets the maximum expected rate of SN II's in a QSO at $\nu = L/E \approx 10$ SN yr^{-1}, i.e., roughly consistent with the required rate.

Alternatively, the mass supply may be long-termed. This could occur if we are seeing the ablation of a stellar atmosphere (Baldwin et al. 1994; Perry & Dyson 1985 or the stripping of a QSO accretion disk due to Kelvin-Helmholtz instability at the boundary between the disk and a fast QSO wind. Baldwin et al. (1994) have suggested that the spectrum of Q0207−398 can be understood as the superposition of a "normal" quasar spectrum and the spectrum of an ablating, dense gas cloud 0.1 pc from the quasar nucleus. In the case of Q0207−398, absorption lines are not seen. Q0059−2735 might be a quasar similar to Q0207−398, but seen through the ablating gas flow.

6. CONCLUSIONS

The bright quasar, Q0059−2735 may become a Rosetta stone for the understanding of the origin of BAL outflow in QSOs. Modeling the rich narrow-line spectrum seen in Q0059−2735 offers an unprecedented opportunity for determining the physical conditions in the absorbing-line gas. The

model can also give the relative abundances of a wide sample of elements in a QSO nucleus. If future observations show changes in the spectrum, our model is so constrained by the observations that we will be able to derive important new information about physical interactions between the quasar radiation field and the circumnuclear gas which gives rise to the BAL phenomenon. The results of the initial analysis discussed in this paper show that NALs including those arising from the excited levels of Fe II, are likely only a few parsecs from the QSO nucleus. These absorption clouds are also closely associated with the low-ionization BAL clouds.

In spite of somewhat different conditions, both types of clouds have a very thin H I layer with ionized column densities exactly equal to the Strömgren column density. The striking result is that the relative thickness of the H I layer is of the order of 10^{-2} N_S. This fact strongly suggests the existence of a fine-tuning mechanism for removal of excessive H I material in the Lyman continuum shadow. The dynamical instability at the H II/H I interface related with the sharp decrease of Lyman continuum is a possible mechanism.

The analysis of the NAL and BAL column densities in terms of photoionization models shows that both absorption features may be reconciled with a single photoionization parameter, $U = 0.2$. The analysis of BAL flow suggests that Fe is possibly overabundant by factor of the order of 10 relative to carbon. The chemical abundance of material so close to a high-redshift quasar nucleus is of great interest and needs to be reexamined using spectra with lower noise than are available to us. Spectra that have higher S/N than ours might also reveal weak lines in the outer halo of Q0059−2735. Such lines could be expected to have nearly the same velocity as the peak of the Mg II emission line—which might represent the intrinsic velocity of Q0059−2735—and be redshifted with respect to the NAL clouds discussed here by ~ 900 km s^{-1}. Also, future observations that cover the spectral range between 3100 and 3600 Å will allow modeling of the important O I and C II absorption lines in Q0059−2735.

The distribution of residual intensities among the high- and low-ionization BAL flows, together with the residual intensity found for the NALs, shows that the low-ionization NAL clouds occult less of the UV continuum source(s) than the BAL flow does. While the low-ionization BAL clouds occult all the continuum source(s), they do not occult the BEL region of the ion producing the BAL. Like the low-ionization BAL clouds, the high-ionization BAL clouds cover the continuum source(s), and in addition, they cover all but the lowest velocity part of their associated BEL. The Q0059−2735 absorption-line system may be created by the evaporation of a low-ionization gas source that has suddenly been placed in the radiation field of a quasar. Possible scenarios include ejection of low-ionization accretion disk material by SN explosions, stand-off shocks around obstacles in the QSO wind, stripping of the disk by a fast QSO wind, or ablation of a stellar envelope(s).

We would like to thank the ESO La Silla night assistants, in particular Jorge Merandez and Manuel Bahamondes for their help. Discussions on Q0207−398 with J. Baldwin and G. Ferland have benefited this paper. This paper has benefited from the many useful suggestions by the referee, who carefully reviewed our manuscript. We are also grateful to Pascal Ballester, Klaus Banse, and Michele Peron for their willing help in modifying the MIDAS programs so that they ran faster and were well adapted to our echelle data reductions. And, finally, we would like to thank Leon Lucy for his suggestions and encouragement.

REFERENCES

Aldrovandi, S. M. V., & Péquignot, D. 1973, A&A, 25, 137
Artymowicz, P., Lin, D. N. C., & Wampler, E. J. 1993, ApJ, 409, 592
Baldwin, J. A., Ferland, G. J., Carswell, R. F., Phillips, M. M., Wilkes, B., & Williams, R. E. 1994, preprint
Begelman, M. C., de Kool, M., & Sikora, M. 1991, ApJ, 382, 416
Chugaĭ, N. 1980, Soviet Astron. Lett., 6, 266
Chugaĭ, N. N. 1992, Soviet Astron., 36, 63
Collin-Souffrin, S., & Dumont, S. 1986, A&A, 166, 13
Collin-Souffrin, S., & Lasota, J. P. 1988, PASP, 100, 1041
de Boer, K. S., Jura, M. A., & Shull, J. M. 1987, in The Scientific Accomplishments of the IUE, ed. Y. Kondon (Dordrecht: Reidel), 485
de Kool, M., & Meurs, E. J. A. 1994, A&A, 281, L65
D'Odorico, S., Pettini, M., & Ponz, D. 1985, ApJ, 299, 852
Fuhr, J. R., Martin, G. A., & Wiese, W. L. 1988, J. Phys. Chem. Ref. Data, 17, Suppl. 4, 108
Gaskell, C. M. 1982, ApJ, 263, 79
Hamann, F., & Ferland, G. 1992, ApJ, 391, L53
Hamann, F., Korista, K. T., & Morris, S. L. 1993, ApJ, 415, 541
Hazard, C., McMahon, R. G., Webb, J. K., & Morton, D. C. 1987, ApJ, 323, 263
Ivanov, V. V. 1973, Transfer of Radiation in Spectral Lines (Washington, DC: NBS)
Kurucz, R. L., & Peytremann, E. 1975, A Table of Semiempirical *gf* Values (SAO Spec. Rep. 362) (Cambridge: Smithsonian Astrophys. Obs.)
Kwan, J. 1990, ApJ, 353, 123
Mathews, W. G., & Ferland, G. J. 1987, ApJ, 323, 456
Matteucci, F., & Padovani, P. 1993, ApJ, 419, 485
Morton, D. C. 1978, ApJ, 222, 863
Morton, D. C., York, D. G., Jenkins, E. B. 1988, ApJS, 68, 449
Netzer, H., & Wills, B. J. 1983, ApJ, 275, 445
Péquignot, D., Aldrovandi, S. M. V., & Stasińska, G. 1978, A&A, 63, 313
Perry, J. J., & Dyson, J. E. 1985, MNRAS, 213, 665
Petitjean, P., Boisson, C., & Péquignot, D. 1990, A&A, 240, 433
Petitjean, P., Rauch, M., & Carswell, R. F. 1994, A&A, 291, 29
Pettini, M., Hunstead, R. W., Murdoch, H. S., & Blades, J. C. 1983, ApJ, 273, 436
Pettini, M., Smith, L. J., Hunstead, R. W., & King, D. L. 1994, ApJ, 426, 79
Reilman, R. F., & Manson, S. T. 1979, ApJS, 40, 815
Scargle, J. D. 1973, ApJ, 179, 705
Scargle, J. D., Caroff, L. J., & Noerdlinger, P. D. 1970, ApJ, 161, L115
Shull, J. M. 1980, ApJ, 237, 769
Shull, J. M., & Van Steenberg, M. 1982, ApJS, 48, 95
Turnshek, D. 1988, in QSO Absorbing Lines: Probing the Universe, ed. J. C. Blades, D. A. Turnshek, & C. A. Norman (Cambridge: Cambridge Univ. Press), 17
Tytler, D., & Fan, X.-M. 1992, ApJS, 79, 1
Voit, G. M., Weymann, R. J., & Korista, K. T. 1993, ApJ, 413, 95
Wampler, E. J., Bergeron, J., & Petitjean, P. 1993, A&A, 273, 15
Weymann, R. J., Morris, S. L., Foltz, C. B., & Hewett, P. C. 1991, ApJ, 373, 23
Wills, B. J., Netzer, H., & Wills, D. 1985, ApJ, 288, 94